is possible only in noncausal systems, we have

$$\mathbf{y}(t) * p(t) = \int_{-\infty}^{\infty} \mathbf{y}(t')p(t - t')\,dt'$$
$$= \int_{-\infty}^{\infty} \mathbf{y}(t')s(t' - t) = \mathbf{y}(t) \star s(t). \tag{3.246}$$

Matched filtering is thus equivalent to correlating the data with the signal we are trying to detect.

Applications of matched filtering are discussed in Chapters 8 and 10.

Wiener-Helstrom Filter

An important variation on the Wiener filter was devised by Helstrom (1967). He considered the problem of estimating a signal that has been corrupted in two ways—by being convolved with a known filter function (usually a blurring or low-pass filter) and by the addition of signal-independent noise. The data to be filtered are of the form

$$\mathbf{y}(t) = [\mathbf{s}(t) * h(t)] + \mathbf{n}(t), \tag{3.247}$$

where $h(t)$ and the autocorrelation functions of $\mathbf{s}(t)$ and $\mathbf{n}(t)$ are presumed known. An estimate $\hat{\mathbf{s}}(t)$ of the signal is to be formed by filtering $\mathbf{y}(t)$ with a filter of impulse response $p(t)$. Again we choose the minimum mean-squared error as the optimality condition.

Helstrom showed that the optimum filter for this problem has a transfer function given by

$$P(\nu) = \frac{H^*(\nu)}{|H(\nu)|^2 + [S_n(\nu)/S_s(\nu)]}. \tag{3.248}$$

Several limits are of interest. First, note that if $h(t) = \delta(t)$, $H(\nu) = 1$, and the original Wiener filter is recovered. Second, if the signal-to-noise ratio is very good at all frequencies, such that $[S_n(\nu)/S_s(\nu)]^2 \ll |H(\nu)|^2$, then $P(\nu)$ reduces to an inverse filter, $P(\nu) = [H(\nu)]^{-1}$. Finally, if the SNR is very poor and both signal and noise are white, then $S_n(\nu)/S_s(\nu)$ is large and constant and the Wiener–Helstrom filter becomes a matched filter $P(\nu) \propto [H(\nu)]^*$.

4

Application of Linear Systems Theory to Radiographic Imaging

4.1 A GENERAL MODEL

It is our goal in this section to devise a simple model that can be used to describe transmission radiography, nuclear scanners, cameras with collimators, and cameras with pinholes. Such a model may seem an unlikely prospect since these systems are quite different in concept, intent, and performance. Nevertheless, as we shall see, the important features of all of them can be discussed within a common framework.

Consider first a simple nuclear pinhole imaging system with the geometry shown in Fig. 4.1. For now the object is assumed to be a planar gamma-ray emitter; the extension to three-dimensional objects can be made later. Additional simplifications concern the pinhole aperture and the detector, both of which are also assumed to be planar. In practice these are reasonable assumptions for very low-energy gamma rays that are absorbed in a small thickness of aperture or detector material. In general, a planar description of the aperture is not valid, since we need to know not only where the photon strikes the aperture plate, but also its angle of incidence to calculate the probability of its being transmitted through to the detector. However, if the absorption coefficient of the aperture material is so high that the aperture plate thickness can be made small compared to the pinhole diameter, then the angle of incidence becomes unimportant and a planar description of the aperture transmission suffices. Similarly, if the detector is either physically

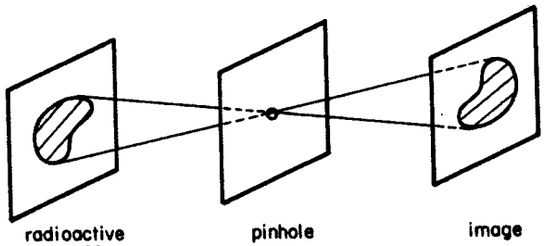

Fig. 4.1 Basic geometry for pinhole imaging of a planar emissive object.

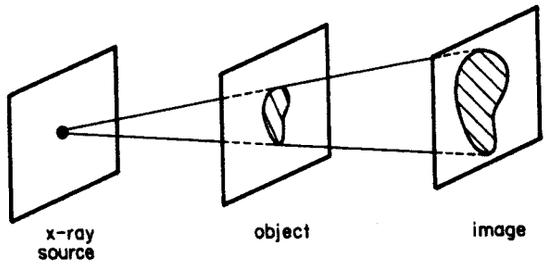

Fig. 4.2 Basic geometry for transmission radiography of a planar object.

thin, or so absorbing that all detection takes place in a thin surface layer, then again a planar description is adequate.

A simple transmission radiography system is shown in Fig. 4.2. The similarity to the pinhole system should be obvious. X rays are generated by electron bombardment of a planar anode, pass through a planar object and impinge on a planar detector. All three planes are assumed to be parallel, although in practice the x-ray anode is usually tipped at an angle to reduce

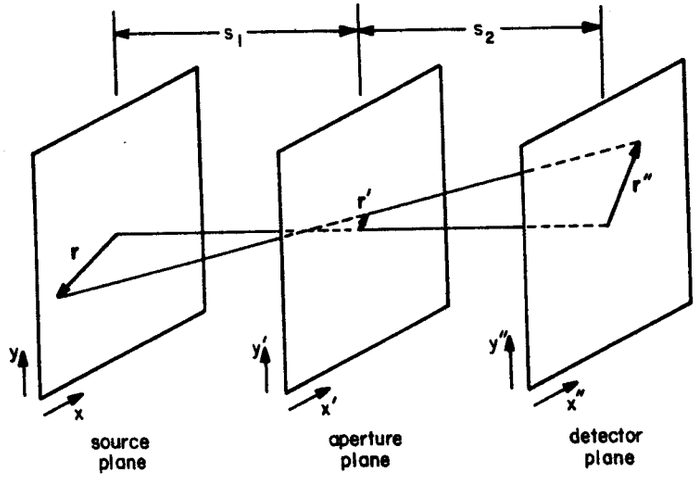

Fig. 4.3 The geometry of a general model for radiographic imaging.

the apparent focal spot size. There are some suspicious features of this model, particularly the planar object. Nevertheless we shall begin our analysis here and let the model gradually become more realistic (and hence more intractable).

The common features of the transmission radiography system and the pinhole camera, as we have modeled them, are thus a source plane, a transmitting or aperture plane, and a detector plane (see Fig. 4.3).

4.1.1 The Source

We describe the source by an *emission function* $f(\mathbf{r})$, where $\mathbf{r}$ is a two-dimensional vector in the source plane. More precisely, $f(\mathbf{r})\,d^2r$ is the *mean* number of photons per unit time emitted into all space from an elemental area d^2r located at the point $\mathbf{r}$. It is important to note that $f(\mathbf{r})$ should really be a statistical quantity. If we observed the system for a finite time T, we would *not* expect to find exactly $Tf(\mathbf{r})\,d^2r$ photons emitted from the element d^2r during the observation. Indeed, the very notion of an infinitesimal number of photons, obtained by multiplying the infinitesimal area d^2r by any finite number, is a contradiction in terms. However, if we repeated the observation many times, or considered an ensemble of many identical x-ray systems, then $Tf(\mathbf{r})\,d^2r$ would represent the average value of all our observations. Deviations from this mean behavior are the subject of Chapter 10; in this chapter all results are to be interpreted as statistical averages.

Of course, $Tf(\mathbf{r})\,d^2r$ represents the mean number of photons emitted from d^2r during the interval T only if $f(\mathbf{r})$ is independent of time. Otherwise a time integral is required. Time-varying sources are occasionally desirable, as with pulsed x-ray tubes, or unavoidable, as with rapidly decaying isotopes. But a time integral would be a distinct nuisance here, so we simply assume it away and take $f(\mathbf{r})$ to be constant in time.

One final comment on $f(\mathbf{r})$ concerns the directional character of the photon emission. If the source is a radionuclide distribution there is no reason to assume any directionality at all. Photons are emitted with equal probability in all directions. The situation is very different with x-ray sources. The bremsstrahlung has a definite preferred orientation which depends on electron energy, angle of electron incidence, and target material. Clearly such complexity is incompatible with a simple model, so once again we ignore it (for now) and consider only isotropic emitters.

4.1.2 The Detector

Having described an elemental source, let us now consider an elemental detector of area $d^2\mathbf{r}''$, where $\mathbf{r}''$ is the two-dimensional position vector in the

detector plane. This elemental detector subtends a solid angle $d\Omega$ from the source, given by

$$d\Omega = \frac{d^2r'' \cdot \cos\theta}{R^2}. \tag{4.1}$$

Referring to Fig. 4.4, we see that R is the distance from source element to detector element and θ is the angle between the normal to the detector surface and the line of sight from source to detector. From simple geometry, we find

$$R = (s_1 + s_2)/\cos\theta, \tag{4.2}$$

so that

$$d\Omega = \frac{\cos^3\theta}{(s_1 + s_2)^2}\, d^2r''. \tag{4.3}$$

If there were no absorbing material in the space between the source plane and the detector plane, the detector would intercept a fraction $d\Omega/4\pi$ of the radiation emitted from any source element since a full sphere subtends 4π steradians. The mean number of photons per unit time emitted by the area element d^2r in the source plane and intercepted by the area element d^2r'' in the detector plane would then be given by

$$f(\mathbf{r})\, d^2r\, \frac{d\Omega}{4\pi} = f(\mathbf{r})\, \frac{\cos^3\theta}{4\pi(s_1 + s_2)^2}\, d^2r\, d^2r''. \tag{4.4}$$

Of course, not all of the photons intercepted by the detector are detected. And even when a photon is detected, its location $\mathbf{r}''$ cannot be measured with absolute accuracy. The detector should, in principle, be considered as an integral part of the imaging system. For now, however, we are concentrating on other portions of the system and may assume an ideal detector. This restriction will be lifted shortly.

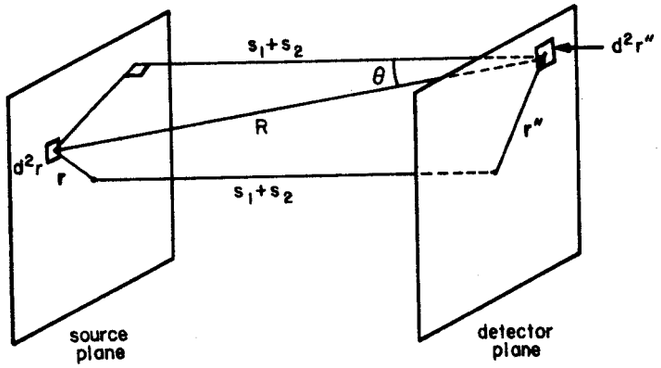

Fig. 4.4 Diagram for solid-angle calculation (aperture plane not shown).

4.1.3 The Transmitting Plane

Our description of the system is nearly complete. We have only to account for the transmitting plane situated between the source and detector. This is easily accomplished since we shall deal only with rays that travel in straight lines; scattered radiation is the subject of another chapter. Thus a ray emanating from the point $\mathbf{r}$ and striking the detector at $\mathbf{r}''$ must have passed through the central plane at a specific point $\mathbf{r}'$ (see Fig. 4.3). We shall denote by $g(\mathbf{r}')$ the transmittance of the central plane at the point $\mathbf{r}'$. In other words, $g(\mathbf{r}')$ is the fraction of the incident photons that is transmitted through the central plane.

We can now write down an expression for the density of detected photons $h(\mathbf{r}'')$, defined so that $h(\mathbf{r}'')\, d^2r''$ is the mean number of photons intercepted by the detector area d^2r'' in a time T. This definition says nothing about where the photon came from, so an integration over the source plane is required:

$$h(\mathbf{r}'')\, d^2r'' = \frac{T\, d^2\mathbf{r}''}{4\pi(s_1 + s_2)^2} \int_{\text{source}} d^2r \cos^3\theta\, f(\mathbf{r}) g(\mathbf{r}'). \tag{4.5}$$

Dimensionally, $h(\mathbf{r}'')$ is a *fluence* as defined in Appendix D. However, the term fluence is more appropriate to a beam of moving particles than to a static pattern of recorded photons. Thus, we shall call $h(\mathbf{r}'')$ a *photon density* rather than a fluence.

The vector $\mathbf{r}'$ can be eliminated in terms of $\mathbf{r}$ and $\mathbf{r}''$. Inspection of the geometry of Fig. 4.3 reveals that

$$\frac{\mathbf{r}' - \mathbf{r}}{s_1} = \frac{\mathbf{r}'' - \mathbf{r}'}{s_2} \tag{4.6}$$

or

$$\mathbf{r}' = \frac{s_2}{s_1 + s_2}\mathbf{r} + \frac{s_1}{s_1 + s_2}\mathbf{r}'' = a\mathbf{r}'' + b\mathbf{r}, \tag{4.7}$$

where

$$a = s_1/(s_1 + s_2) \tag{4.8}$$

and

$$b = s_2/(s_1 + s_2) = 1 - a. \tag{4.9}$$

Some care must be taken in interpreting (4.6) or (4.7) since $\mathbf{r}$, $\mathbf{r}'$, and $\mathbf{r}''$ are all two-dimensional vectors defined in different planes. If $\mathbf{r}$ has Cartesian components (x, y) and $\mathbf{r}'$ has components (x', y'), then by $\mathbf{r}' - \mathbf{r}$ we mean a two-dimensional vector with components $(x' - x, y' - y)$. The z dimension

does not influence this vector difference. The three-dimensional distance R is not simply $|\mathbf{r} - \mathbf{r}''|$, but is given by

$$R = [|\mathbf{r} - \mathbf{r}''|^2 + (s_1 + s_2)^2]^{1/2}$$
$$= [(x - x'')^2 + (y - y'')^2 + (s_1 + s_2)^2]^{1/2}. \tag{4.10}$$

In spite of this complication, the notation is still intended to be suggestive. Note that if all figures are drawn so that the radiation goes from left to right, then the letters representing the important functions (f, g, and h) progress from left to right, the number of primes on the coordinates ($\mathbf{r}, \mathbf{r}', \mathbf{r}''$) increases from left to right, and the designations for both absolute spacings (s_1 and s_2) and relative spacings (a and b) increase from left to right.

Equation (4.5) now becomes

$$h(\mathbf{r}'')\,d^2r'' = C\,d^2r' \int_{\text{source}} d^2r \cos^3\theta\, f(\mathbf{r})g(a\mathbf{r}'' + b\mathbf{r}), \tag{4.11}$$

where

$$C = T[4\pi(s_1 + s_2)^2]^{-1}. \tag{4.12}$$

This equation is still rather complicated since θ is a function of $\mathbf{r}$ and $\mathbf{r}''$. However, we shall often be interested in systems, where $s_1 + s_2$ is large compared to $|\mathbf{r}|$ or $|\mathbf{r}''|$. In those cases it is a good approximation to take $\theta \approx 0$ and $\cos^3\theta \approx 1$. We are then left with

$$h(\mathbf{r}'') \approx C \int_{\text{source}} d^2r\, f(\mathbf{r})g(a\mathbf{r}'' + b\mathbf{r}), \tag{4.13}$$

where the factor d^2r'', originally inserted for didactic purposes, has been dropped from both sides of the equation.

4.1.4 Reduction to a Convolution

Equation (4.13) now resembles a convolution integral. To exploit this resemblance, let us define a new variable $\mathbf{r}_0''$, given by

$$\mathbf{r}_0'' = -b\mathbf{r}/a \tag{4.14}$$

and scaled versions of f and g by

$$\tilde{f}(\mathbf{r}_0'') = f(\mathbf{r}) = f(-a\mathbf{r}_0''/b) \tag{4.15}$$

and

$$\tilde{g}(\mathbf{r}_0'') = g(a\mathbf{r}_0''). \tag{4.16}$$

We then have

$$g(a\mathbf{r}'' + b\mathbf{r}) = g(a\mathbf{r}'' - a\mathbf{r}_0'') = \tilde{g}(\mathbf{r}'' - \mathbf{r}_0''). \tag{4.17}$$

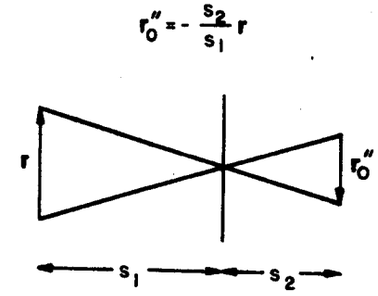

Fig. 4.5 Illustration of the significance of $\mathbf{r}_0''$ in (4.14).

The significance of the variable $\mathbf{r}_0''$ is illustrated in Fig. 4.5. Multiplication of the vector $\mathbf{r}$, which is measured in the source plane, by $-b/a$ (or, equivalently, $-s_2/s_1$) is the same as projecting it through a point in the aperture plane to the image plane. Similar geometric interpretations may be attached to the scaled functions $\tilde{f}$ and $\tilde{g}$. As Fig. 4.6 shows, $g(a\mathbf{r}'')$ is *wider* than $g(\mathbf{r}'')$ since the scale factor a is less than one. The scaled function $\tilde{g}(\mathbf{r}'')$ may be thought of as the original aperture function $g(\mathbf{r}')$ projected from a point in the source plane to the image plane. By the same token, $\tilde{f}(\mathbf{r}'')$ is the original source function projected through a point in the aperture plane to the image plane. The tilde will always imply projection *to the image plane.*

After these manipulations (4.13) may be written

$$h(\mathbf{r}'') = \left(\frac{a}{b}\right)^2 C \int_\infty d^2r_0''\, \tilde{f}(\mathbf{r}_0'')\tilde{g}(\mathbf{r}'' - \mathbf{r}_0'')$$
$$= (a/b)^2 C\tilde{f}(\mathbf{r}'') ** \tilde{g}(\mathbf{r}''). \tag{4.18}$$

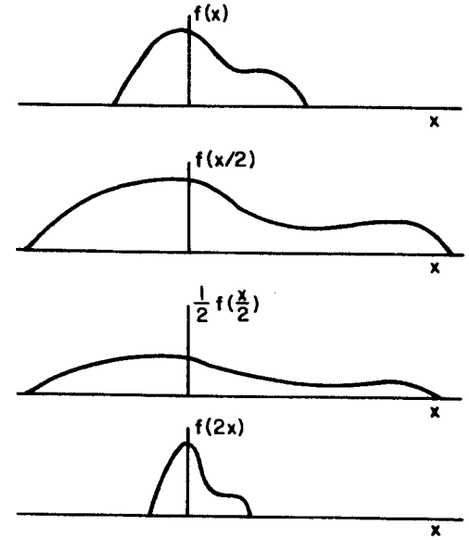

Fig. 4.6 Illustration of scaled functions. Note that $f(ax)$ is wider than $f(x)$ if $a < 1$ and narrower than $f(x)$ if $a > 1$. Note also that $af(ax)$ and $f(x)$ yield the same value when integrated over x.

(The domain of the $\mathbf{r}_0''$ integration may be taken as the entire two-dimensional space, indicated by the subscript ∞ on the integral sign, since f, and hence $\tilde{f}$, vanishes outside a finite area.) In other words, the detected photon density may be thought of as the output of a two-dimensional linear system with input $\tilde{f}$ and impulse response proportional to $\tilde{g}$. As in any linear system, a frequency-domain description is very useful. A straightforward two-dimensional Fourier transform of (4.18) yields

$$\mathcal{F}_2\{h(\mathbf{r}'')\} = H(\boldsymbol{\rho}'') = (a/b)^2 C\tilde{F}(\boldsymbol{\rho}'')\tilde{G}(\boldsymbol{\rho}''), \tag{4.19}$$

where $\boldsymbol{\rho}''$ is the spatial frequency vector conjugate to $\mathbf{r}''$ in the image plane. The transform on the right of this equation may be evaluated in terms of the original source and transmission functions f and g by use of the scaling relation (B.94):

$$\tilde{F}(\boldsymbol{\rho}'') = \mathcal{F}_2\{f(-a\mathbf{r}''/b)\} = (b^2/a^2)F(-b\boldsymbol{\rho}''/a) \tag{4.20}$$

and

$$\tilde{G}(\boldsymbol{\rho}'') = \mathcal{F}_2\{g(a\mathbf{r}'')\} = (1/a^2)G(\boldsymbol{\rho}''/a). \tag{4.21}$$

Our final result is then

$$H(\boldsymbol{\rho}'') = (C/a^2)F(-b\boldsymbol{\rho}''/a)G(\boldsymbol{\rho}''/a). \tag{4.22}$$

Application of the basic equations (4.18) and (4.22) to various imaging systems is the subject of the remainder of this chapter.

4.2 PINHOLE IMAGING

A pinhole camera is the simplest possible imaging system. Its major features can be determined from elementary geometry without resort to the elaborate mathematics unveiled in the Section 4.1. Our goal in this section is therefore not to use the mathematics to understand the pinhole camera, but rather the reverse—to use the pinhole camera to demystify the mathematics.

4.2.1 Geometrical Treatment

Consider an ideal pinhole aperture that is perfectly transmitting over a small circular region of diameter d'_{ph}, and perfectly opaque elsewhere, so that

$$g(\mathbf{r}') = \text{circ}(2r'/d'_{\text{ph}}) = \begin{cases} 1 & \text{if } 2r'/d'_{\text{ph}} < 1 \\ 0 & \text{if } 2r'/d'_{\text{ph}} > 1, \end{cases} \tag{4.23}$$

where $r' \equiv |\mathbf{r}'|$. The prime on d'_{ph} indicates that it is measured in the $\mathbf{r}'$ plane.

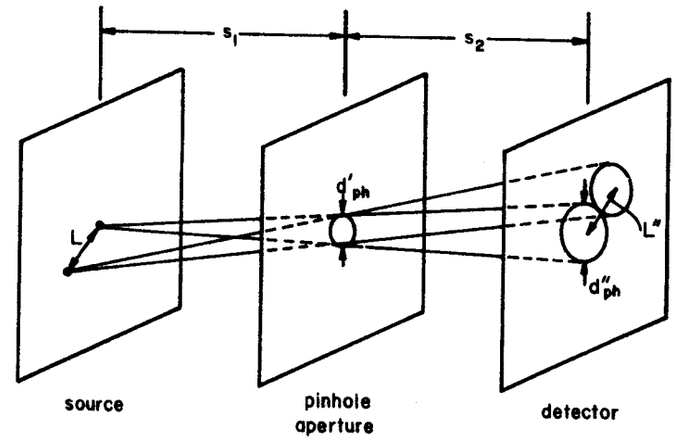

Fig. 4.7 Diagram illustrating the calculation of the point spread function for pinhole imaging.

Suppose that the source is a single emissive point. Then, since the rays must travel in straight lines, the image consists of a collection of detected photons confined to a circular region of diameter d''_{ph} (see Fig. 4.7). By comparing similar triangles, we see that

$$d''_{\text{ph}} = d'_{\text{ph}} \frac{s_1 + s_2}{s_1} = \frac{d'_{\text{ph}}}{a}. \tag{4.24}$$

Note that the value of d''_{ph} is completely independent of the position of the source. No matter what the projection angle θ is, the circular pinhole always projects to an undistorted circular image provided the aperture plane is parallel to the detector plane. In brief, the system is shift-invariant.

If we consider two point sources a distance L apart, inspection of Fig. 4.7 shows that the centers of their images in the r'' plane are separated by a distance L'' given by

$$L'' = L(s_2/s_1) = L(b/a). \tag{4.25}$$

Furthermore, the image is inverted; we say that the pinhole camera has a magnification of $-b/a\ (= -s_2/s_1)$.

4.2.2 Analytical Treatment

The results of the geometrical analysis also follow easily from (4.18). We describe a point source at the location $\mathbf{r}_s$ as a delta function, i.e.,

$$f^{\delta}(\mathbf{r}) = K\,\delta(\mathbf{r} - \mathbf{r}_s), \tag{4.26}$$

where the superscript δ reminds us we are dealing with a point source, and K is the *total* number of photons per unit time emitted by the source. Note that this definition is consistent with the interpretation of $\tilde{f}(\mathbf{r})$ as the number of emitted photons per unit time per unit area since, by the definition of the delta function,

$$\int_{\text{source}} f^{\delta}(\mathbf{r})\, d^2r = K \int_{\text{source}} \delta(\mathbf{r} - \mathbf{r}_s)\, d^2r = K. \tag{4.27}$$

The scaled functions $\tilde{f}(\mathbf{r})$ and $\tilde{g}(\mathbf{r})$ that appear in (4.18) may be written

$$\tilde{f}^{\delta}(\mathbf{r}'') = K\,\delta[(-a\mathbf{r}''/b) - \mathbf{r}_s] = K(b^2/a^2)\,\delta[\mathbf{r}'' + (b\mathbf{r}_s/a)] \tag{4.28}$$

and

$$\tilde{g}(\mathbf{r}'') = \text{circ}(2a\mathbf{r}''/d'_{\text{ph}}), \tag{4.29}$$

where use has been made of the scaling property of delta functions, (A.37), to obtain the right-hand form of (4.28). Equation (4.18) itself is now

$$\begin{aligned} h^{\delta}(\mathbf{r}'') &= KC \int_{\infty} d^2r''_0\, \delta\left(\mathbf{r}''_0 + \frac{b\mathbf{r}_s}{a}\right) \text{circ}\left(\frac{2a|\mathbf{r}'' - \mathbf{r}''_0|}{d'_{\text{ph}}}\right) \\ &= KC\,\text{circ}\left(\frac{2a|\mathbf{r}'' + (b\mathbf{r}_s/a)|}{d'_{\text{ph}}}\right). \end{aligned} \tag{4.30}$$

We next seek to persuade the reader that the circ function in this equation describes the same magnified pinhole image that we deduced on geometrical grounds. First, note that the center of the circ function is located at the value of $\mathbf{r}''$ that makes the argument of the function zero. This occurs when $\mathbf{r}'' = -b\mathbf{r}_s/a$, in agreement with the geometrical picture. Let $\mathbf{r}''_s$ be defined as the coordinate of the center of the circ function, i.e.,

$$\mathbf{r}''_s = -b\mathbf{r}_s/a. \tag{4.31}$$

The circ function of (4.30) vanishes unless its argument is less than 1, or

$$|\mathbf{r}'' - \mathbf{r}''_s| < \frac{d'_{\text{ph}}}{2a} = \frac{d'_{\text{ph}}}{2}\frac{s_1 + s_2}{s_1}. \tag{4.32}$$

This inequality will hold provided $\mathbf{r}''$ lies within a circle of diameter d'_{ph}/a $(= d''_{\text{ph}})$ centered at $\mathbf{r}''_s$. Thus, once again the geometrical result is confirmed.

Equation (4.30) not only gives the right functional form for $h(\mathbf{r}'')$, but also the right magnitude. To see this, note that the disk of diameter d'_{ph}/a in the detector plane subtends a solid angle Ω (as seen from the source plane) given by

$$\Omega = \frac{\pi(d'_{\text{ph}}/a)^2}{4(s_1 + s_2)^2}. \tag{4.33}$$

The total number of detected photons in time T is thus the total number emitted KT times the fractional solid angle $\Omega/4\pi$. But $h(\mathbf{r}'')$ is the detected photon *density*. Within the disk region, $h(\mathbf{r}'')$ is the total number collected divided by the area of the disk, i.e.,

$$h^{\delta}(\mathbf{r}'') = \frac{KT\Omega/4\pi}{\pi(d'_{\text{ph}}/a)^2/4} = \frac{KT}{4\pi(s_1 + s_2)^2}, \qquad [|\mathbf{r}'' - \mathbf{r}''_s| < d'_{\text{ph}}/2a], \tag{4.34}$$

which, with the definition of C from (4.12), is in perfect accord with (4.30).

4.2.3 Resolution

Either the geometrical or the mathematical approach can be used to determine the resolution distance of the system, i.e., the minimum resolvable spacing of two point sources. The only real problem is specifying what we mean by "minimum resolvable." One possibility would be to adopt the full width at half-maximum (FWHM) of the PSF as our resolution criterion. In the present case, the PSF as measured in the image plane is a uniform disk of diameter d''_{ph}; the FWHM of this function is therefore also d''_{ph}. This criterion would thus not count two points as resolved unless their separation was such that there was no overlap at all between the two disk images. This may seem to be an overly stringent condition. Surely an observer would have no difficulty in asserting that two points were present if the centers of their images were separated by, say $\frac{1}{2}d''_{\text{ph}}$. Indeed, many writers adopt this condition in discussing the resolution of a pinhole camera. Nevertheless, we believe that the FWHM criterion is defensible in most practical circumstances. Unfortunately, the defense rests largely on noise considerations and must therefore be postponed to Chapter 10. For now, we simply adopt the FWHM criterion without real justification. The reader who objects to this choice can sprinkle around factors of order unity to taste.

Our criterion thus says that the centers of the *images* of the two points must be separated by d''_{ph} for the points to be resolved. Of more interest, however, is how far apart *the points themselves* must be. In other words, we are more concerned with the PSF scaled to the actual size of the object than with the PSF as it appears in the image plane. This is an easy scaling since we have already determined that the magnification of the pinhole camera is $-b/a$ (or $-s_2/s_1$). For two points to be barely resolved (by the FWHM criterion), they must be separated in the object plane by a distance δ_{ph}, given by

$$\delta_{\text{ph}} = d''_{\text{ph}}a/b = d'_{\text{ph}}/b = d'_{\text{ph}}(s_1 + s_2)/s_2. \tag{4.35}$$

To be more formal about it, the PSF of the pinhole camera is the measured point-source image $h^{\delta}(\mathbf{r}'')$ rescaled to account for the magnification,

and normalized to unit source strength, i.e.,

$$\begin{aligned}\mathrm{PSF}_{\mathrm{ph}} = p_{\mathrm{ph}}(\mathbf{r}-\mathbf{r}_s) &= K^{-1}(b/a)^2 h^{\delta}(\mathbf{r}'')\big|_{\mathbf{r}''=-b\mathbf{r}/a} \\ &= C\left(\frac{b}{a}\right)^2 \mathrm{circ}\left(\frac{2b|\mathbf{r}-\mathbf{r}_s|}{d'_{\mathrm{ph}}}\right),\end{aligned} \tag{4.36}$$

which has a FWHM of d'_{ph}/b, in agreement with (4.35). The scaling must involve the amplitude as well as the lateral dimensions of the function. The leading factor of b^2/a^2 in (4.36) is required so that the total number of photons will be conserved, i.e., the integral of $p_{\mathrm{ph}}(\mathbf{r})$ over the $\mathbf{r}$ plane will be identical to the integral of $h^{\delta}(\mathbf{r}'')$ over the $\mathbf{r}''$ plane. The reader may verify that the constants in (4.36) are reasonable by showing that the integral of $p_{\mathrm{ph}}(\mathbf{r})$ is simply $\Omega T/4\pi$. Notice that $p_{\mathrm{ph}}(\mathbf{r})$ has units of time per length squared, so that $p_{\mathrm{ph}}(\mathbf{r}) ** f(\mathbf{r})$ represents the mean number of *collected* photons per unit area in the rescaled image.

4.2.4 Modulation Transfer Function

The MTF of the pinhole camera may be found, as usual, by Fourier transforming the PSF. The details of the transform are given in Appendix B;

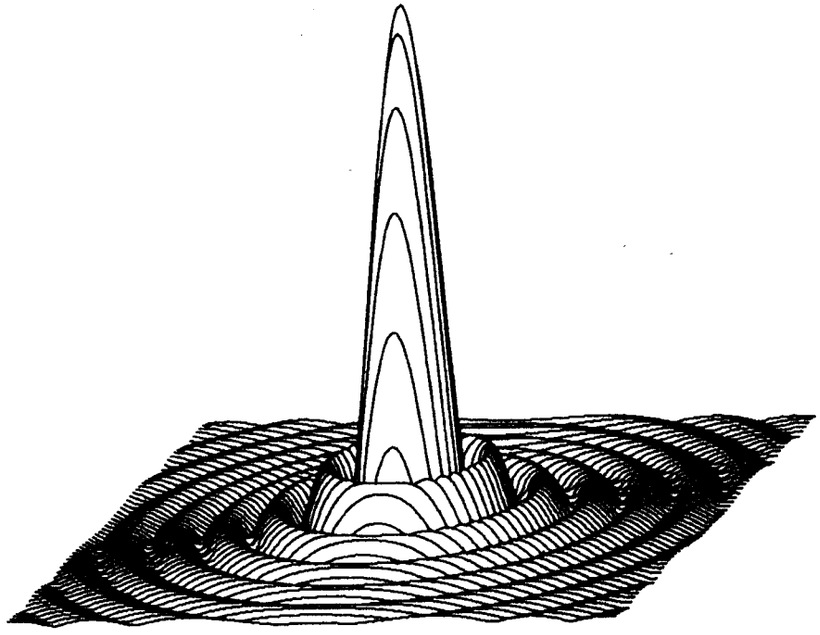

Fig. 4.8 Isometric plot of the function $2J_1(\alpha\rho)/\alpha\rho$.

by (B.114), the result is

$$\mathrm{MTF}_{\mathrm{ph}} = \frac{|P_{\mathrm{ph}}(\rho)|}{P_{\mathrm{ph}}(0)} = \frac{|2J_1(\pi d'_{\mathrm{ph}}\rho/b)|}{\pi d'_{\mathrm{ph}}\rho/b} \tag{4.37}$$

where, as in Chapter 2, ρ is the magnitude of the two-dimensional spatial-frequency vector, and $J_1(\ )$ is the first-order Bessel function of the first kind. The function $2J_1(\alpha\rho)/\alpha\rho$ is the two-dimensional, circularly symmetric counterpart of the sinc function defined in (2.58). It is sometimes referred to as a "Besinc" function or, in the southwest, as a "sombrero" function (see Fig. 4.8). However, since the usage is not yet standardized, we shall refrain from giving this function a name.

4.2.5 The Image Detector

Since the PSF (or the transfer function) is a complete specification of a linear, shift-invariant system, it would seem that we have completed the analysis of the pinhole camera. However, we have not yet included the effects of the image detector. The problem is closely akin to the cascaded linear systems discussed in Chapter 2. The first system is the image-forming pinhole aperture. Its input is the two-dimensional source density $f(\mathbf{r})$, and its output is the photon density incident on the detector $h(\mathbf{r}'')$. If the detector were ideal, its output would be just proportional to $h(\mathbf{r}'')$. Real detectors, however, further degrade the image and must be treated as linear systems in their own right.

Cascaded linear systems are most easily analyzed in the frequency domain. The input signal to the detector system is thus given by $H(\boldsymbol{\rho}'')$, the Fourier transform of $h(\mathbf{r}'')$. The transfer function of the detector will be denoted by $D(\boldsymbol{\rho}'')$, so the detector output is simply $D(\boldsymbol{\rho}'')H(\boldsymbol{\rho}'')$. With the aid of (4.22), this becomes

$$D(\boldsymbol{\rho}'')H(\boldsymbol{\rho}'') = (C/a^2)D(\boldsymbol{\rho}'')F(-b\boldsymbol{\rho}''/a)G(\boldsymbol{\rho}''/a). \tag{4.38}$$

This equation may appear strange at first since the three functions on the right all have different scale factors. But bear in mind that we are really interested in how a particular spatial-frequency component *in the object* is affected by the cascaded system. It is quite irrelevant to us whether the final image is displayed at a large scale or a small one. What we must do, therefore, is to rewrite this equation so that the object transform $F(\boldsymbol{\rho})$ appears without any scale factors. The coefficient of $F(\boldsymbol{\rho})$ will then be the overall transfer function of the cascaded system, referred back to the original object scale.

To accomplish this, we merely let $\boldsymbol{\rho} = -b\boldsymbol{\rho}''/a$ in (4.38). The result is

$$D(-a\boldsymbol{\rho}/b)H(-a\boldsymbol{\rho}/b) = (C/a^2)D(-a\boldsymbol{\rho}/b)F(\boldsymbol{\rho})G(-\boldsymbol{\rho}/b). \tag{4.39}$$

Reading off the coefficient of $F(\rho)$, we obtain the transfer function of the total system, pinhole plus detector,

$$TF_{tot} = P_{tot}(\rho) = (C/a^2)D(-a\rho/b)G(-\rho/b). \tag{4.40}$$

Note that no modification of the leading constant is necessary when rescaling functions in the frequency domain. The central ordinate theorem (B.96) guarantees that the left-hand side of (4.40), when transformed back to the space domain, will have the same spatial integral as before scaling. The factor of b^2/a^2 introduced into (4.36) is automatically taken into account in (4.40).

An inverse transform now gets us back to the space domain and to an expression for the PSF of the total system:

$$\mathrm{PSF}_{tot} = p_{tot}(\mathbf{r}) = (C/a^2)\mathscr{F}_2^{-1}\{D(-a\rho/b)G(-\rho/b)\}. \tag{4.41}$$

This function can be broken down into its component parts by use of the convolution theorem (B.52). We then obtain

$$p_{tot}(\mathbf{r}) = p_{ph}(\mathbf{r}) ** p_{det}(\mathbf{r}), \tag{4.42}$$

where $p_{ph}(r)$ is the PSF due to the pinhole alone [cf. (4.36)] as given by

$$p_{ph}(\mathbf{r}) = (C/a^2)\mathscr{F}_2^{-1}\{G(-\rho/b)\} = (Cb^2/a^2)g(-b\mathbf{r}). \tag{4.43}$$

Similarly, $p_{det}(\mathbf{r})$ is the contribution of the detector to the overall PSF and is given by

$$p_{det}(\mathbf{r}) = \mathscr{F}_2^{-1}\{D(-a\rho/b)\} = (b/a)^2 d(-b\mathbf{r}/a). \tag{4.44}$$

Note that p_{det} has dimensions of $(\text{area})^{-1}$ even though p_{ph} has dimensions of time per area. Note also that an ideal detector, for which $D(\rho'') = 1$ at all frequencies, leads to $p_{det}(\mathbf{r}) = \delta(\mathbf{r}) \equiv (b^2/a^2)\,\delta(-b\mathbf{r}/a)$.

It is also important to keep in mind that we are referring all PSFs to a common scale—the scale of the original object in the $\mathbf{r}$ plane. The notation $p_{det}(\mathbf{r})$ does *not* mean the PSF *of* the detector; it means the contribution of the detector to the overall PSF as measured in the object plane. The PSF of the detector, as measured in the detector plane, is just $d(\mathbf{r}'')$. The scale factors in (4.44) serve to project this function through a point in the aperture plane to the object or source plane. On the other hand, we had to originally have $h(\mathbf{r}'')$ expressed in the $\mathbf{r}''$ plane in order to regard it as the input to the detector. Only after the cascading expressed in (4.38) was it correct to rescale the results to the $\mathbf{r}$ plane.

4.2.6 Design Considerations

We next inquire how these results might be used to design a pinhole camera. The parameters at our disposal are the spacings s_1 and s_2 and the diameter of the pinhole. It is assumed that the size and MTF of the detector

are fixed, and that we must image an object of a specified size. Within these constraints, we must optimize the resolution and the gamma-ray collection efficiency of the pinhole camera.

The first constraint to apply is the required size of the object field (field of view, or FOV for short). If the detector is circular with diameter d''_{det}, and the object lies within a circular region of diameter d_{ob}, which is large compared to δ_{ph}, then the entire object can be imaged if

$$d''_{det} \geq \frac{s_2}{s_1} d_{ob} = \frac{b}{a} d_{ob}. \tag{4.45}$$

In other words, the magnified object must fit on the detector.

Equation (4.45) is not the only constraint on s_1/s_2; the resolution distance δ_{ph} also depends on that parameter. Inspection of (4.35) shows that δ_{ph} takes on its minimum of d'_{ph} when $s_1/s_2 \to 0$.

Of course, (4.35) was derived on the assumption of an ideal detector, but the same conclusion follows when a realistic detector is considered—the best resolution is obtained with the smallest s_1/s_2. Qualitatively, the degradation due to the detector is least serious when the image is greatly magnified since then the width of the detector PSF is a small fraction of the image size. More quantitatively, our goal is to make the detector's contribution to the transfer function, $D(-a\rho/b)$ in (4.40), as large as possible. Since D will generally decrease as the spatial frequency is increased, we must make the magnitude of the argument of D, i.e., the quantity $|-a\rho/b|$, as small as possible at all frequencies. This can occur only if a/b is small. To restate the argument in the space domain, the function $d(-b\mathbf{r}/a)$ in (4.44) falls to one-half its peak value when the argument of the function equals some specified value, call it $\mathbf{r}_{1/2}$. The FWHM of $p_{det}(\mathbf{r})$ is then given by $2(a/b)r_{1/2}$. The parameter $r_{1/2}$ is a characteristic of the detector and presumably beyond our control. The only way to minimize the FWHM of $p_{det}(\mathbf{r})$ is thus to minimize a/b.

Of course, a/b cannot be made arbitrarily small, since then (4.45) would be violated and the FOV would be inadequate. The smallest allowed a/b is the value for which (4.45) becomes an equality rather than an inequality, i.e., $a/b = d_{ob}/d''_{det}$.

To this point, we have fixed a/b, or s_1/s_2, but not s_1 and s_2 separately; the total source-detector distance $s_1 + s_2$ is still a free parameter. It is clear from (4.3) that $s_1 + s_2$ should be small in order to efficiently collect photons [note that the factor $(s_1 + s_2)^{-2}$ appears either explicitly or implicitly though the constant C in all of our imaging equations]. There is, however, a penalty to be paid if $s_1 + s_2$ is made too small. The problem lies in the obliquity factor $\cos^3\theta$ that last appeared in (4.11). The subsequent treatment was based on the approximation $\cos^3\theta \approx 1$, an approximation that breaks down for large objects and small spacings. The planar model for the aperture can also break down under these same conditions. The upshot is that gamma rays

are collected less efficiently from the periphery of the object plane than from the center; a uniform object produces an image that is less intense at the edges (see Fig. 4.9). The system designer must decide how much of this shading can be tolerated and set $s_1 + s_2$ accordingly.

An additional consideration affecting the choice of $s_1 + s_2$ arises when three-dimensional objects are considered. In that case, s_1 is a variable specifying depth within the object. If the pinhole is close to the surface of the object, then the magnification and the collection efficiency will both vary rapidly with depth in the object. Therefore, both lateral spatial dimensions and intensities will be distorted, possibly confusing the diagnostic process. A value judgment, not readily amenable to quantification, is required to set tolerable bounds on these distortions.

The last parameter we must consider is d'_{ph}. Once again a trade-off is involved—a large d'_{ph} will increase collection efficiency but degrade spatial resolution. In general, determination of just where to set this trade-off is an extraordinarily difficult problem that ultimately comes down to the psychophysical question: Does the human observer perform better with a sharp, noisy image or with a blurred but less noisy one? We do not propose to answer this question in this book, although some possible approaches to the

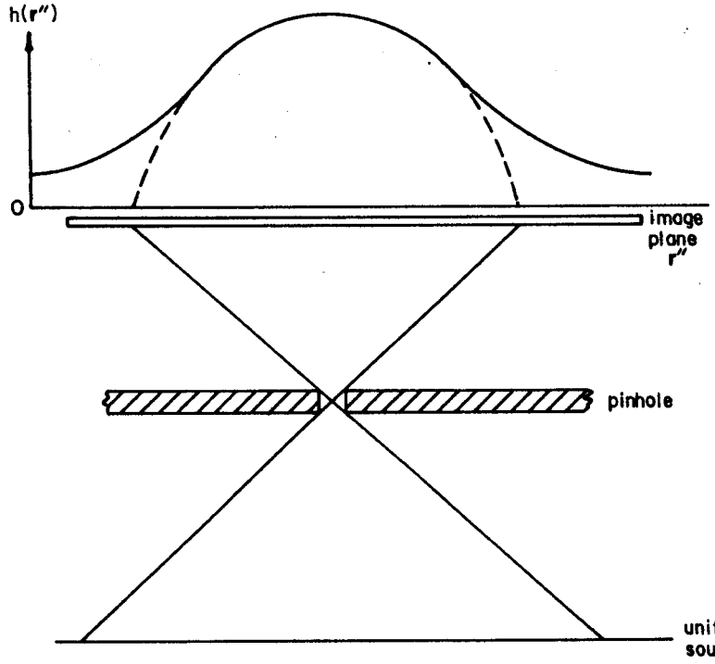

Fig. 4.9 Illustration of image shading due to obliquity and vignetting in the pinhole camera. Solid line: obliquity alone. Dashed line: obliquity plus vignetting. For this drawing, the pinhole material is assumed to be perfectly opaque.

problem are briefly discussed in Chapter 10. Even if we confined our attention to purely physical measures of image quality, we could not give a very complete discussion at this point because we have not yet included noise in our formulation. Therefore, we shall postphone the discussion of this problem until Chapter 10. For now, it is sufficient to bear in mind that radiological images in general, and nuclear pinhole images in particular, are almost always severely limited by the small number of detected photons. Collection efficiency is of paramount importance.

4.3 TRANSMISSION RADIOGRAPHY

It is a simple matter to recast the pinhole-imaging equations into a form applicable to transmission radiography. The basic difference is that in the pinhole case the source function $f(\mathbf{r})$ represents the object being imaged, and the aperture function $g(\mathbf{r}')$ is under the control of the system designer. The reverse is true in transmission imaging where $g(\mathbf{r}')$ represents the object and $f(\mathbf{r})$ is the more-or-less controllable focal spot of the x-ray tube (Ter-Pogossian, 1967; Rossmann, 1968, 1969; Doi, 1965; Doi and Rossman, 1975).

4.3.1 Disk Focal Spot

To accentuate the similarity, let us suppose that the focal spot is a uniform, emissive disk of diameter d_{fs}, i.e.,

$$f(\mathbf{r}) = f_0 \operatorname{circ}(2r/d_{fs}), \tag{4.46}$$

where f_0 is the emission density (photons per unit area per unit time) within the disk region (see Fig. 4.10).

To find the PSF of the system, we must consider the input to be a point object described by

$$g^{\delta}(\mathbf{r}') = \delta(\mathbf{r}' - \mathbf{r}'_1). \tag{4.47}$$

where $\mathbf{r}'_1$ is the location of the point in the $\mathbf{r}'$ plane. This input function may offend the reader's intuition somewhat since $g(\mathbf{r}')$ is supposed to represent a transmission, which is a dimensionless number in the range 0–1. The unit-impulse transmission $g^{\delta}(\mathbf{r}')$, on the other hand, has dimensions of $(\text{length})^{-2}$ (see Appendix A) and has a peak value of infinity rather than unity. If a mental picture is required, one can imagine a pinhole aperture whose area is allowed to approach zero while the exposure time is increased in inverse proportion to the area, so that the total x-ray flux transmitted through the pinhole during the exposure is constant. This metaphor corresponds to the notion of a point source, which we viewed as a very small, very bright source.

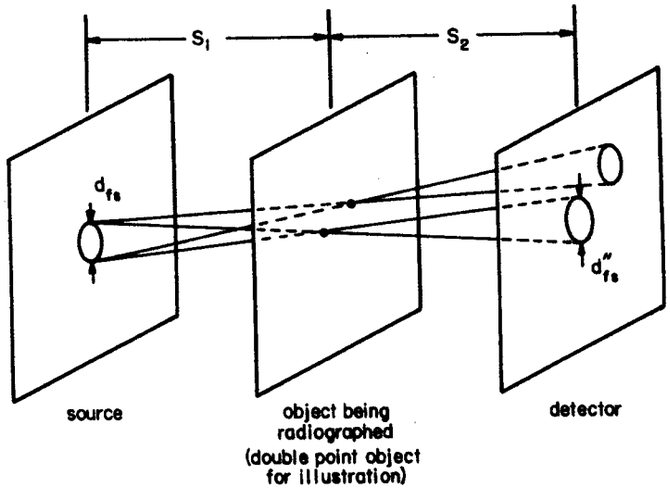

Fig. 4.10 Diagram illustrating the calculation of the point spread function for transmission radiography with a disklike focal spot.

In the limit, it became infinitesimally small and infinitely bright in such a way that the total number of emitted photons remained constant. In the transmission case, the object becomes "infinitely transmissive" over an infinitesimal area.

We can now see that the PSF of the transmission radiography system, as measured in the detector plane, is simply the pinhole image of the focal spot. Substituting (4.46) and (4.47) into (4.13), we find

$$\begin{aligned} h^{\delta}(\mathbf{r}'') &= C \int_{\text{source}} d^2r\, f_0 \operatorname{circ}\left(\frac{2r}{d_{fs}}\right) \delta(a\mathbf{r}'' + b\mathbf{r} - \mathbf{r}'_1) \\ &= \left(\frac{C}{b^2}\right) f_0 \operatorname{circ}\left[\frac{2|a\mathbf{r}'' - \mathbf{r}'_1|}{bd_{fs}}\right] \\ &= \left(\frac{C}{b^2}\right) f_0 \operatorname{circ}\left[\frac{2|\mathbf{r}'' - (\mathbf{r}'_1/a)|}{bd_{fs}/a}\right]. \end{aligned} \tag{4.48}$$

This equation describes a uniform disk image of diameter d''_{fs}, given by

$$d''_{fs} = d_{fs}\frac{s_2}{s_1} = d_{fs}\frac{b}{a}. \tag{4.49}$$

The disk is centered at $\mathbf{r}'' = \mathbf{r}'_1/a = \mathbf{r}'_1(s_1 + s_2)/s_1$; the magnification m_t is therefore $(s_1 + s_2)/s_1$. Note that the magnification is always greater than one and that it is a positive number. The image inversion encountered in the pinhole camera does not occur here.

Two points are said to be just resolvable, on the FWHM criterion, if the center-to-center spacing of their images is equal to d''_{fs}. As in the pinhole

camera case, we then scale the spacing back to the object plane (in this case, the $\mathbf{r}'$ plane) by dividing by the magnification. Formally, we set $d''_{fs} = r'_1/a$ and solve for r'_1, which is then identified as the resolution distance δ'_{fs}. (The subscript fs indicates that we are considering only the contribution of the focal spot to the resolution, and the prime shows that the resolution is measured in the $\mathbf{r}'$ plane.) The result is

$$\delta'_{fs} = d_{fs}b = d_{fs}\frac{s_2}{s_1 + s_2}. \tag{4.50}$$

The symmetry between (4.50) and (4.35) should not be overlooked. One is obtained from the other by transposing the object dimension and the resolution-determining system parameter (d_{fs} or d'_{ph}).

4.3.2 General Analysis

We may generalize our description to include an arbitrary focal-spot distribution and also include the effect of the detector by again using (4.38). This time, however, $G(\boldsymbol{\rho}''/a)$ represents the object. Since we are interested in how a particular spatial-frequency component in the object is affected by the system, we must rescale (4.38) so that $G(\boldsymbol{\rho}')$ appears on the right-hand side. To accomplish this, we let $\boldsymbol{\rho}' = \boldsymbol{\rho}''/a$ in (4.38). The result is

$$D(a\boldsymbol{\rho}')H(a\boldsymbol{\rho}') = (C/a^2)D(a\boldsymbol{\rho}')F(-b\boldsymbol{\rho}')G(\boldsymbol{\rho}'). \tag{4.51}$$

This is the transmission-imaging counterpart of (4.39). The coefficient of $G(\boldsymbol{\rho}')$ is the overall transfer function of the system:

$$TF_{\text{tot}} = P_{\text{tot}}(\boldsymbol{\rho}') = \frac{C}{a^2} D(a\boldsymbol{\rho}')F(-b\boldsymbol{\rho}'). \tag{4.52}$$

Returning to the space domain, we find that the overall PSF is given by

$$\begin{aligned} \text{PSF}_{\text{tot}} &= p_{\text{tot}}(\mathbf{r}') = \frac{C}{a^2}\mathscr{F}_2^{-1}\{D(a\boldsymbol{\rho}')F(-b\boldsymbol{\rho}')\} \\ &= p_{fs}(\mathbf{r}') ** p_{\text{det}}(\mathbf{r}'), \end{aligned} \tag{4.53}$$

where $p_{fs}(\mathbf{r}')$ is the PSF due to the focal spot alone,

$$p_{fs}(\mathbf{r}') = \frac{C}{a^2}\mathscr{F}_2^{-1}\{F(-b\boldsymbol{\rho}')\} = \left(\frac{C}{a^2b^2}\right) f\left(\frac{-\mathbf{r}'}{b}\right). \tag{4.54}$$

The detector contribution to the PSF is

$$p_{\text{det}}(\mathbf{r}') = \mathscr{F}_2^{-1}\{D(a\boldsymbol{\rho}')\} = (1/a^2)\, d(\mathbf{r}'/a). \tag{4.55}$$

Note that the scaling factors in this equation are different from those in the pinhole case [cf. (4.44)] even though the same symbol $p_{det}(\mathbf{r}')$ is used. Note also that both p_{fs} and p_{tot} have dimensions of (length)$^{-4}$, in contrast to p_{ph} which had dimensions of time per (length)^2. However, p_{fs} is to be convolved with a dimensionless quantity, a transmission, to get the image h, while p_{ph} is to be convolved with a source density having dimensions (length)$^{-2}$ · (time)$^{-1}$. Thus in both cases, h has dimensions (length)$^{-2}$ and represents the mean number of photons per unit area in the image.

4.3.3 Design Considerations

With these basic equations, we are now in a position to discuss the design tradeoffs in transmission imaging. The first thing we shall discover is that there is an optimum magnification even if there is no limitation imposed by the finite detector size. This is in marked contrast to the pinhole camera case where we found that the magnification should be as large as possible. A large magnification (small s_1/s_2) served to minimize the widths of both $p_{ph}(\mathbf{r})$ and $p_{det}(\mathbf{r})$. In the transmission case, on the other hand, a large magnification ameliorates the detector contribution to the overall blur but exacerbates the focal spot contribution. To see this, recall that the magnification m_t is given by

$$m_t = \frac{1}{a} = \frac{1}{1-b}, \tag{4.56}$$

or

$$b = 1 - \frac{1}{m_t} = \frac{m_t - 1}{m_t}. \tag{4.57}$$

Therefore,

$$p_{fs}(\mathbf{r}') \propto f\left(\frac{-m_t\mathbf{r}'}{m_t - 1}\right), \tag{4.58}$$

and

$$p_{det}(\mathbf{r}') \propto d(m_t\mathbf{r}'). \tag{4.59}$$

The width of $p_{fs}(\mathbf{r}')$ is the smallest when the coefficient of $\mathbf{r}'$ in the argument of (4.58) is the largest, which occurs when $m_t = 1$. This corresponds to the "contact print" limit when the detector is in direct contact with the object being radiographed. In that case the size of the focal spot is irrelevant and a sharp shadow is always cast on the detector. Of course, this limit may not be physically possible, as when the object of interest lies deep within the patient's body. Nor is it necessarily desirable to have a contact print when the detector limitations are considered. Just as in the pinhole case, a large magnification serves to minimize the width of $p_{det}(\mathbf{r}')$, a result that should be readily evident from (4.59).

An explicit solution for the optimum magnification is possible when both the detector and the focal spot can be represented as Gaussian functions—always a convenient mathematical artifice and occasionally a realistic one as well. The problem is easiest in the frequency domain. Therefore let us assume that

$$D(\boldsymbol{\rho}'') \propto \exp[-\pi(\rho''/\rho_d'')^2] \tag{4.60}$$

and

$$F(\boldsymbol{\rho}) \propto \exp[-\pi(\rho/\rho_f)^2], \tag{4.61}$$

where ρ_d'' and ρ_f are characteristic widths of the MTF of the detector and focal spot, respectively. From (4.52), we find for the overall MTF,

$$\mathrm{MTF}_{tot} = \frac{|P_{tot}(\boldsymbol{\rho}')|}{P_{tot}(0)} = \exp[-\pi(a\rho'/\rho_d'')^2]\exp[-\pi(b\rho'/\rho_f)^2] \tag{4.62}$$

By virtue of (4.56) and (4.57),

$$\mathrm{MTF}_{tot} = \exp\left[-\pi\rho'^2\left(\frac{1}{(m_t\rho_d'')^2} + \frac{(m_t-1)^2}{m_t^2\rho_f^2}\right)\right]. \tag{4.63}$$

The width of MTF_{tot} will be an extremum if

$$\frac{d}{dm_t}\left[\frac{1}{(m_t\rho_d'')^2} + \frac{(m_t-1)^2}{m_t^2\rho_f^2}\right] = 0, \tag{4.64}$$

which has the solution

$$m_t^{opt} = 1 + (\rho_f/\rho_d'')^2. \tag{4.65}$$

It is easily verified that the extremum corresponds to a maximum width for MTF_{tot} and hence an optimum configuration as implied by the superscript.

The behavior of (4.65) in two limits is of interest. First, note that a very large focal spot ($\rho_f \to 0$) requires the contact-print configuration, $m_t = 1$. Second, a very poor detector ($\rho_d'' \to 0$) requires large magnification.

As with the pinhole camera, an additional design consideration arises when we consider the finite detector area. This problem is relatively unimportant when x-ray film or a film-screen system is used since a large area is easy to obtain. With x-ray image intensifiers, on the other hand, the detector area is very limited, which is unfortunate since the MTF is also relatively poor and (4.65) shows that a large magnification is desirable.

4.3.4 Realistic Focal Spots

While some x-ray tubes do have focal spots that approximate Gaussian functions, they are the exception rather than the rule. A more realistic focal spot is illustrated in Fig. 4.11, and its associated MTF is shown in Fig. 4.12.

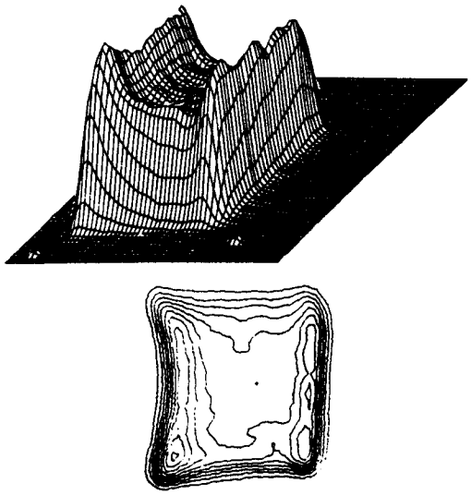

Fig. 4.11 Pinhole image of an actual x-ray tube focal spot, isometric and contour representations. (From Wagner *et al.*, 1974.)

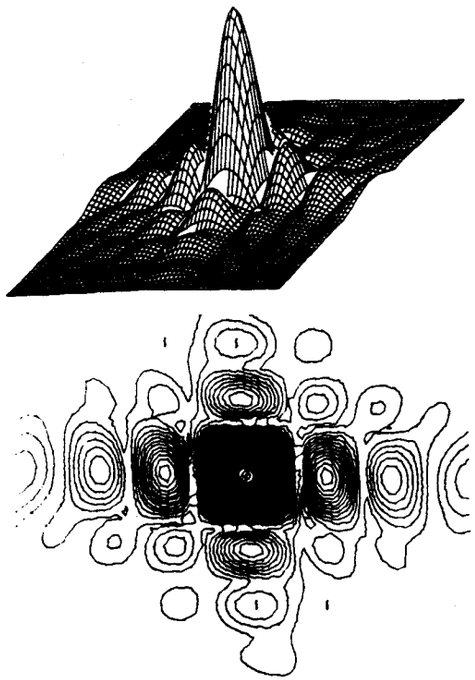

Fig. 4.12 MTF obtained with the focal spot shown in Fig. 4.11, isometric and contour representations. (From Wagner *et al.*, 1974.)

Many attempts have been made to reduce these complicated functions to single numbers—something akin to our d_{fs} in (4.46) or ρ_f in (4.61). Frequently, manufacturers and medical physicists will differ by as much as a factor of 3 when asked to specify the "effective focal spot size" of a given x-ray tube. We do not propose to enter this rather sterile debate. Suffice it to say that the complete PSF or transfer function is required to properly specify the characteristics of the focal spot; any lesser description provides less information.

One qualitative difference between the Gaussian focal spot and the realistic one in Fig. 4.11 concerns the phase of the transfer function. A Gaussian transfer function has zero phase at all spatial frequencies, which is seldom true with realistic focal spots. The existence of these phase shifts is revealed in a radiograph of a bar target as shown in Fig. 4.13. The origin of

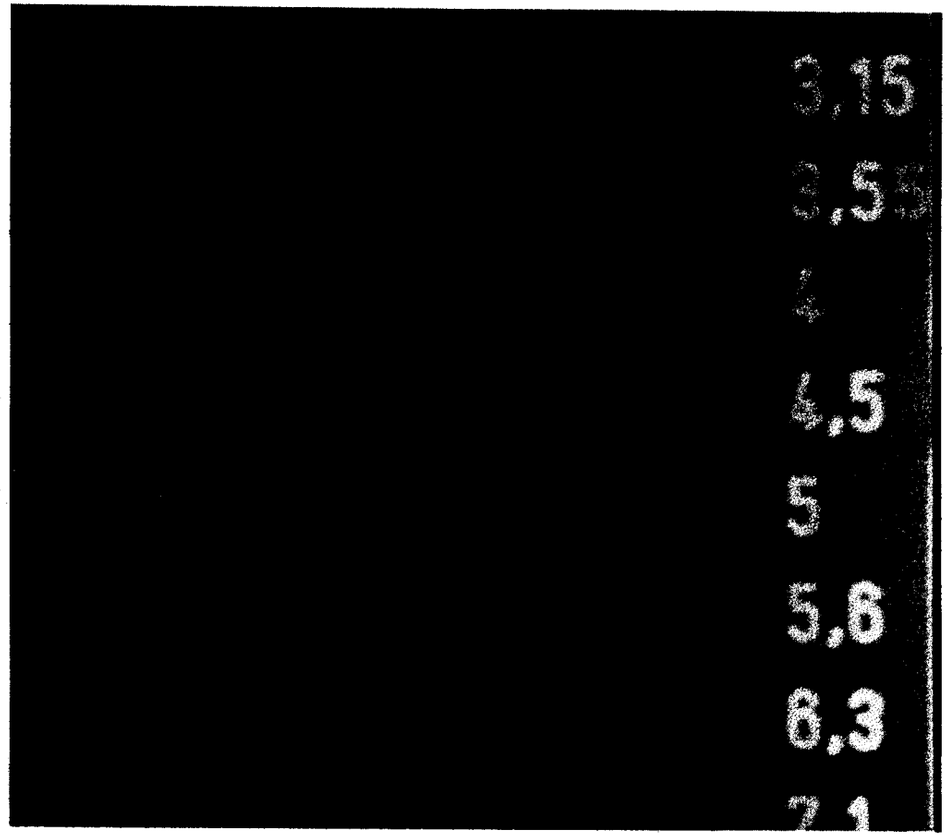

Fig. 4.13 Radiograph of a bar target illustrating phase shifts. Note that the modulation of the bars vanishes at 4.5 lp/mm, and that the phase of the modulation at lower frequencies is opposite that at the higher frequencies. (Courtesy of Meryll Frost.)

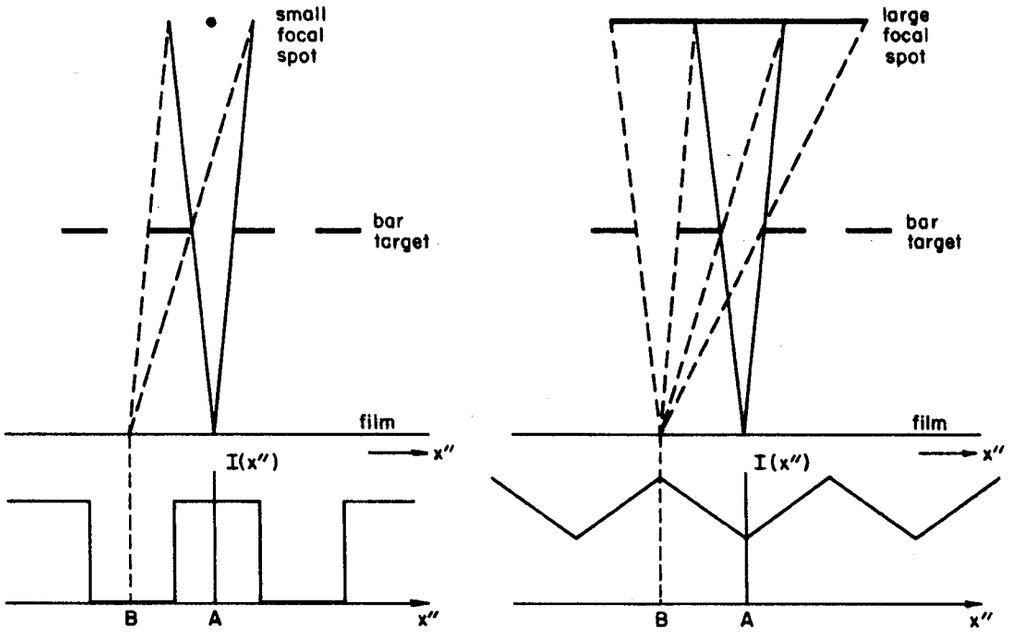

Fig. 4.14 Geometric explanation of the origin of the phase shifts seen in Fig. 4.13. At left, a small focal spot gives a sharp shadow and 100% modulation. The maximum intensity is at point *A*, and the intensity at point *B* is zero. At right, point *A* "sees" only half as much of the large square focal spot as point *B* does. Thus, the intensity at *B* is twice as large as at *A*, which is now a *minimum* instead of a maximum.

the reversals can be seen from the geometric construction given in Fig. 4.14.

Our discussion of transmission radiography to this point is by no means complete. We are, however, approaching the limits of what can be learned from a linear, shift-invariant model. We therefore conclude this section here, but we shall return to the subject of transmission imaging in Section 4.8 where the various factors that invalidate our simple model are discussed.

4.4 SCANNERS

Our ultimate goal for this section is to give a fairly rigorous analysis of a a scanner incorporating a multihole focused collimator of the type illustrated in Fig. 1.19 (Barber, 1973; Beck, 1964a,b, 1968b). However, much insight can be gained by starting with a decidedly nonrigorous analysis of a scanner using a single-bore collimator.

4.4.1 Definition of PSF

In order to calculate the PSF of a scanner, we must first state just what we mean by PSF in this case. A rather obvious definition would take the PSF to be the instantaneous count rate of the detector, considered as a function of the position of a point source. There are two difficulties with this definition. The first is that the term "instantaneous count rate" must be understood in a statistical average sense. If the same measurement is repeated many times, or an ensemble of identical systems is considered, then the count rate of concern is $\Delta\bar{N}_c/\Delta t$, where $\Delta\bar{N}_c$ is the mean number of photons detected in a vanishingly small time interval Δt. Of course, in real life one does not have an ensemble of identical systems at his disposal, nor does he normally have the opportunity to repeat the measurement many times. A single measurement over a very small Δt would probably yield only zero or one detected photon and give practically no information about the mean rate. Some sort of averaging is clearly required.

In a practical scanner, this problem is solved by use of a count-rate meter which can take one of several forms. An idealized count-rate meter was discussed in Chapter 3, but a more practical form is the *RC* network shown in Fig. 4.15. The operation of this circuit will be discussed more fully in Section 4.4.7, but for now we simply note that it serves to average the count-rate over a time interval R_1C_1 which is under the operator's control. It might seem that a large value of R_1C_1 would be desirable since then the measured count rate would be an accurate estimate of the instantaneous rate defined above. However, we must not forget that the scanner is moving. A long averaging time will blur the point image in the direction of the scan. The count-rate meter is not just an optional accessory; it is an integral part of the scanner and makes its own contribution to the overall PSF. A full analysis of a scanner must, therefore, include a calculation of both the collimator and ratemeter contributions to the PSF. We shall accomplish both in due course (Beck, 1968a,b; Rao and Wagner, 1967; Mozley, 1968).

The second difficulty with defining the PSF as an instantaneous count rate is that it is dimensionally inconsistent with the definition of PSF used

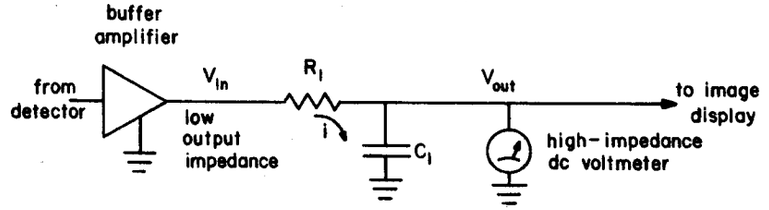

Fig. 4.15 Simple count-rate meter for use with a rectilinear scanner.

in the pinhole imaging discussion. In that case, we arranged for the detected photon density (i.e., the number detected per unit area) to be the emission function $f(\mathbf{r})$ convolved with the PSF. This required the PSF to have dimensions of time per unit area. Since the number of detected photons per unit area will be a key parameter when we come to a discussion of noise, it is highly desirable to standardize our definitions in such a way that this parameter is easy to calculate.

In a scanner, the conversion from counts (detected photons) per unit time to counts per unit area must involve two mechanical parameters, viz., the linear scan speed v_s and the number of scan lines per unit length (in the direction perpendicular to the rapid scan). The latter parameter will be denoted by n_l. Straightforward dimensional analysis then shows that the number of counts per unit area is the instantaneous count rate times n_l/v_s. (The scan lines are assumed to be contiguous and have width $1/n_l$, and v_s is assumed to be constant. Furthermore, no consideration is given to the behavior at the end of a raster line where the direction of scan is reversed.) We shall include this factor n_l/v_s in our definition of PSF for the scanner.

4.4.2 Geometrical Analysis of the PSF of a Single-Bore Collimator

Consider the geometry shown in Fig. 4.16 where a collimator of constant bore diameter D_b and bore length L_b is viewing a point source a distance z from the face of the collimator. In practice, the collimator will usually be scanned in a rectilinear raster over the source. For ease of analysis, however,

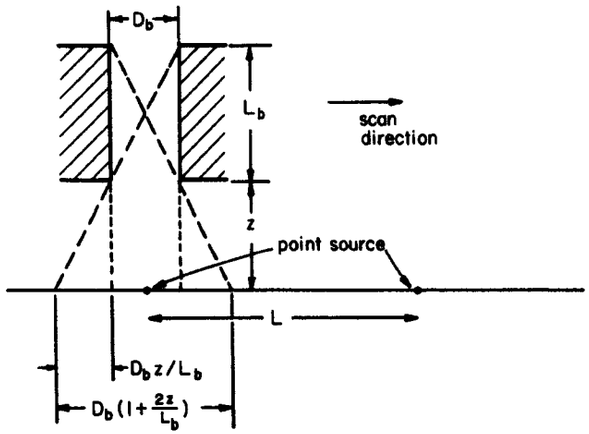

Fig. 4.16 Geometry for the calculation of the PSF of a single-bore collimator.

we assume that the collimator is stationary and the source is scanned; only relative motion is important, so this procedure is still quite general.

A great deal can be learned about the collimator PSF without elaborate calculations. To illustrate, consider first the case $z = 0$, where the source point is virtually in contact with the face of the collimator. Then, assuming there is no penetration of the gamma rays through the walls of the collimator, the count rate must be zero when the point source lies outside the disk region of diameter D_b directly in front of the bore. Furthermore, since L_b will normally be much larger than D_b, the collection solid angle will, to a good approximation, be independent of the location of the point within the disk region. (This approximation is nothing more than a restatement of the $\cos^3\theta \approx 1$ condition that we have been using all along.) Finally, note that the scanner has a magnification of one since the count rate will be a maximum when the collimator is positioned directly over the point source. To image a second point source a lateral distance L away, the collimator must be moved by L. Of course, the final image can be *displayed* at any desired magnification, but this is of no concern since we shall always refer the PSF back to the scale of the object anyway. The main point here is that the magnification inherent in the gamma-ray collection system, in contrast to that obtained with a pinhole, is unity.

With these simple observations, we can now write down an expression for the PSF of the single-bore collimator:

$$\mathrm{PSF}_{sb}(z=0) = p_{sb}(\mathbf{r}; z=0) = \mathrm{const} \cdot \mathrm{circ}(2r/D_b). \tag{4.66}$$

The vector $\mathbf{r}$, of course, represents the two-dimensional position of the point in the plane $z = 0$; the collimator is assumed to be centered on $\mathbf{r} = 0$.

To fix the constant in (4.66), consider a point source emitting K photons per second. Its emission density function is $K\,\delta(\mathbf{r})$ and the instantaneous count rate within the disk region is $K\Omega/4\pi$, where Ω is the solid angle subtended by the detector. The PSF must thus satisfy

$$p_{sb}(\mathbf{r}; z=0) ** K\,\delta(\mathbf{r}) = \frac{n_l}{v_s} \cdot \frac{K\Omega}{4\pi}\ \mathrm{circ}\left(\frac{2r}{D_b}\right). \tag{4.67}$$

Since the solid angle in this case is $\pi D_b^2/4L_b^2$, the PSF is given by

$$p_{sb}(\mathbf{r}; z=0) = \frac{n_l}{v_s} \cdot \frac{D_b^2}{16L_b^2} \cdot \mathrm{circ}\left(\frac{2r}{D_b}\right). \tag{4.68}$$

Note that p_{sb} has dimensions of time per area, so that we can directly convolve p_{sb} with $f(\mathbf{r})$ to get the number of detected photons per unit area. It is not necessary to insert an exposure time T as we did in the pinhole camera and transmission radiography cases.

The general behavior of $p_{sb}(\mathbf{r}; z)$ for $z \neq 0$ is also easy to determine. We need to distinguish three regions in the source plane. The first, which we shall call the *umbra* by analogy with lunar eclipses, is the disk-shaped region of diameter D_b directly in line with the collimator bore. (The term "umbra" is a decided misnomer here since the detector is completely *un*obscured by the walls of the collimator in this region; we could call it an inverse umbra or negative umbra, but let's not be any more pedantic than necessary.) The PSF in the umbra region is approximately constant.

The second region to be discussed will be termed the *penumbra*. It is the region between the umbra and a circle of diameter $D_b[1 + (2z/L_b)]$ as shown in Fig. 4.16. In this region, part of the detector is obscured by the collimator, reducing the collection solid angle and hence the PSF. In the third region, outside the circle of diameter $D_b[1 + (2z/L_b)]$, all of the detector is obscured and the PSF is zero (again neglecting penetration of gamma rays through the collimator).

From these considerations, we can sketch the PSF for any z. In Fig. 4.17 we show the image of two well-resolved point sources. The sloping lines in the penumbra region have been drawn as straight, but the more careful analysis to be given below will show that they have a slight curvature. It should also be kept in mind that we have not yet discussed the effect of the count-rate meter. The image shown in Fig. 4.17 is that which would be obtained with an infinitesimally slow scan.

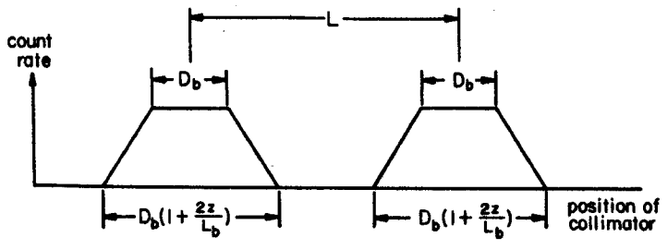

Fig. 4.17 Image of two points with a single-bore collimator.

4.4.3 Analytical Treatment of the Single-Bore Collimator

To complete the analysis of the single-bore collimator we must find an analytical expression for $p_{sb}(\mathbf{r}; z)$ for $z \neq 0$ and Fourier transform it to find the MTF. For this purpose, we again invoke the general model set up in Section 4.1. To show the correspondence between the model and the present problem, we note that the collimator can be replaced by a pair of thin

apertures as shown in Fig. 4.18. If the apertures are made of a hypothetical material that is absolutely opaque to gamma rays, then the aperture pair is equivalent* to the collimator. (The collimator material is also still being treated as impenetrable.)

With this equivalence, the problem closely resembles the pinhole camera problem. One important difference, however, arises because the pinhole aperture is used with an *imaging* detector that measures the coordinates of each gamma ray impinging on it. The scanner detector, on the other hand, is a spatially *integrating* detector that simply counts all gamma rays incident on it, irrespective of their coordinates. The only position dependence is imposed by the upper aperture in Fig. 4.18; a photon is counted only if it falls within the transparent area of that aperture.

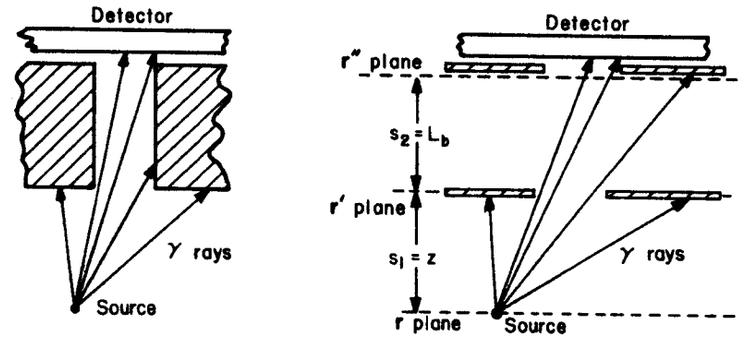

Fig. 4.18 Diagram showing the equivalence between a single-bore collimator and a pair of circular apertures. Left: actual collimator. Right: equivalent apertures.

We can apply the pinhole-camera equations to the single-bore collimator by taking the $\mathbf{r}''$ plane to be just in front of the upper aperture as shown in Fig. 4.18. The function $h(\mathbf{r}'')$ then specifies the photon density incident on the upper aperture. The lower aperture, whose transmission we shall designate $g_1(\mathbf{r}')$, plays the role of the pinhole. The source-to-aperture spacing s_1 then corresponds to z, while the aperture-to-detector distance s_2 is L_b. The

* To be completely realistic, we should admit that there is one type of event for which the two geometries are not exactly equivalent. A gamma ray incident on the wall of the collimator can be either Compton scattered or photoelectrically absorbed. In either case a lower-energy photon is produced, and there is some small probability that it will escape from the wall and strike the detector. In practice, such events will usually be rejected by the pulse height analyzer.

In the equivalent aperture geometry, the collimator walls are not present, so a photon which would strike the wall instead strikes the underside of the upper aperture. The scattered x ray is then shielded from the detector and is not counted even without a pulse height analyzer.

function $h(\mathbf{r}'')$ is given by (4.13), which in the present notation becomes

$$h(\mathbf{r}'') = C \int_\infty f(\mathbf{r}) g_1(a\mathbf{r}'' + b\mathbf{r})\, d^2r, \tag{4.69}$$

where

$$a = z/(L_b + z), \qquad b = L_b/(L_b + z). \tag{4.70}$$

However $h(\mathbf{r}'')$ is the number of photons per unit area in an observation time T. For scanner problems we are often more interested in the number per unit area per unit time. Therefore we define a *flux density* or *fluence rate* by

$$\dot{h}(\mathbf{r}'') \equiv \frac{h(\mathbf{r}'')}{T} = \dot{C} \int_\infty f(\mathbf{r}) g_1(a\mathbf{r}'' + b\mathbf{r}) d^2r, \tag{4.71}$$

where

$$\dot{C} = C/T = [4\pi(L_b + z)^2]^{-1}. \tag{4.72}$$

Since the two apertures are identical and have diameter D_b, we may write

$$g_i(\mathbf{r}') = \text{circ}(2\mathbf{r}'/D_b), \qquad i = 1 \text{ or } 2. \tag{4.73}$$

By retaining two separate subscripts, we may easily generalize the results later so that they apply to a collimator with a tapered bore.

The instantaneous count rate is found by multiplying the photon flux density incident on the upper aperture, $\dot{h}(\mathbf{r}'')$, by the transmission of that aperture, $g_2(\mathbf{r}'')$, and integrating over $\mathbf{r}''$, i.e.,

$$\begin{aligned} \text{count rate} &= \int_\infty \dot{h}(\mathbf{r}'') g_2(\mathbf{r}'') d^2r'' \\ &= \dot{C} \int_\infty d^2r'' \int_\infty d^2r\, f(\mathbf{r}) g_1(a\mathbf{r}'' + b\mathbf{r}) g_2(\mathbf{r}''). \end{aligned} \tag{4.74}$$

We may take the domains of both integrations to be infinite planes since $f(\mathbf{r})$ and $g_2(\mathbf{r}'')$ are zero outside a finite region. To calculate the PSF, we let $f(\mathbf{r})$ be the point source $\delta(\mathbf{r} - \mathbf{r}_s)$. The integration over $\mathbf{r}$ in (4.74) is now trivial, and we find for the PSF

$$\begin{aligned} p_{sb}(\mathbf{r}_s; z) &= \frac{n_i \dot{C}}{v_s} \int_\infty d^2r''\, g_2(\mathbf{r}'') g_1(a\mathbf{r}'' + b\mathbf{r}_s) \\ &= \frac{n_i \dot{C}}{v_s} \int_\infty d^2r'' \,\text{circ}\left(\frac{2r''}{D_b}\right) \text{circ}\left(\frac{2|a\mathbf{r}'' + b\mathbf{r}_s|}{D_b}\right) \\ &= \frac{n_i \dot{C}}{v_s} \int_\infty d^2r'' \,\text{circ}\left(\frac{2r''}{D_b}\right) \text{circ}\left[\frac{2a|\mathbf{r}'' + (b\mathbf{r}_s/a)|}{D_b}\right]. \end{aligned} \tag{4.75}$$

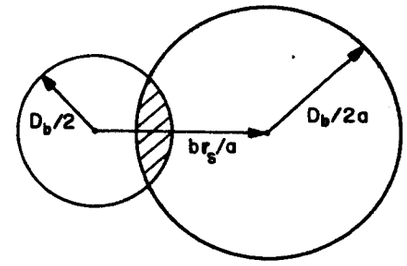

Fig. 4.19 Diagram to aid in interpreting Eq. (4.75).

The integrand in this equation is a product of a circ function of diameter D_b with a second circ function of diameter D_b/a as illustrated in Fig. 4.19; since the parameter a is less than one, the second circ function is larger than the first. The interpretation of this result is that the larger circ function represents the lower aperture as projected from the source point onto the upper aperture. The PSF is proportional to the area of overlap between the two circ functions, or the portion of the detector that can be seen from the source location.

Examine (4.75) in the limit $z \to 0$, or equivalently, $a \to 0$ and $b \to 1$. Then the first circ function is much smaller than the second and may be treated as a delta function:

$$\text{circ}\left(\frac{2r''}{D_b}\right) \approx \frac{\pi D_b^2}{4} \delta(\mathbf{r}''), \tag{4.76}$$

where the constant $\pi D_b^2/4$ is necessary so that both sides of this equation will have the same integral over $\mathbf{r}''$. This approximation allows us to perform the integral in (4.75) with the result

$$p_{sb}(\mathbf{r}_s; z = 0) = \left(\frac{n_i \dot{C}}{v_s}\right) \frac{\pi D_b^2}{4} \text{circ}\left(\frac{2r_s}{D_b}\right), \tag{4.77}$$

which agrees with (4.68) since $\dot{C} = (4\pi L_b^2)^{-1}$ if $z = 0$.

At this point we can drop the subscript s denoting source point on $\mathbf{r}_s$ and refer to the PSF as $p_{sb}(\mathbf{r}; z = 0)$. There are two justifications for this step. The first is that we can call the argument of a function whatever we please so long as we are consistent. But the more important reason is that we shall want to use $p_{sb}(\mathbf{r}, z = 0)$ in convolutions that are carried out in the $\mathbf{r}$ plane. Recall that in the usual definition of the PSF for a shift-invariant imaging system, $p(\mathbf{r})$ represents the response at some image point due to the source point a vector distance $\mathbf{r}$ away. In the above development, the image point was at the collimator location—the origin of coordinates—and the source point was at $\mathbf{r}_s$. The vector $\mathbf{r}_s$ thus has the same meaning as the usual vector $\mathbf{r}$ in $p(\mathbf{r})$.

The behavior of $p_{sb}(\mathbf{r}; z)$ for nonzero values of z is illustrated in Fig. 4.20. Note the curvature of the sloping edges in the penumbra region.

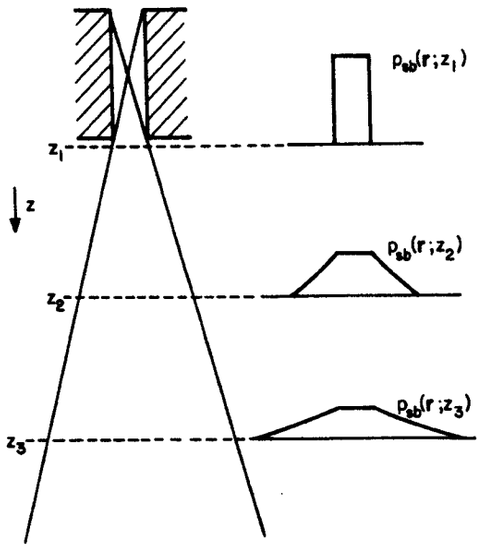

Fig. 4.20 PSF of a single-bore collimator for various values of z, the distance from the source plane to the collimator face.

4.4.4 Modulation Transfer Function

The MTF is proportional to the Fourier transform of (4.75). To perform this transform, it is convenient to first finagle the equation into the form of a convolution. The required manipulations are similar, but not identical, to those carried out in Section 4.1.4. As before, we define

$$\tilde{g}_1(\mathbf{r}'') = g_1(a\mathbf{r}'') \tag{4.78}$$

so that

$$g_1(a\mathbf{r}'' + b\mathbf{r}) = \tilde{g}_1[(b/a)\mathbf{r} + \mathbf{r}'']. \tag{4.79}$$

Equation (4.75) then becomes

$$p_{sb}(\mathbf{r}; z) = (n_i \dot{C}/v_s)[g_2(\mathbf{r}'') ** \tilde{g}_1(\mathbf{r}'')]_{\mathbf{r}''=-b\mathbf{r}/a}. \tag{4.80}$$

The MTF appropriate to the plane z is now readily found by use of (B.52), (B.94), and (B.114). The result is

$$\mathrm{MTF}_{sb} = \frac{|P_{sb}(\boldsymbol{\rho}; z)|}{P_{sb}(0; z)} = \left|\frac{2J_1(\pi a D_b \rho/b)}{\pi a D_b \rho/b}\right| \cdot \left|\frac{2J_1(\pi D_b \rho/b)}{\pi D_b \rho/b}\right|. \tag{4.81}$$

The $z = 0$ limit is again of some interest. In that limit $a \to 0$ and $b \to 1$. Then, since

$$\lim_{X \to 0} [2J_1(X)/X] = 1, \tag{4.82}$$

we find

$$\lim_{z \to 0} \mathrm{MTF}_{sb} = |2J_1(\pi D_b \rho)/\pi D_b \rho|. \tag{4.83}$$

This result could, of course, have been obtained directly by transforming (4.68). Note that it depends on only the bore diameter D_b and on no other geometrical parameter.

4.4.5 The Focused Collimator

Extension of our previous results to the case of a focused collimator (Fig. 4.21) is rather straightforward since each bore can be treated separately.

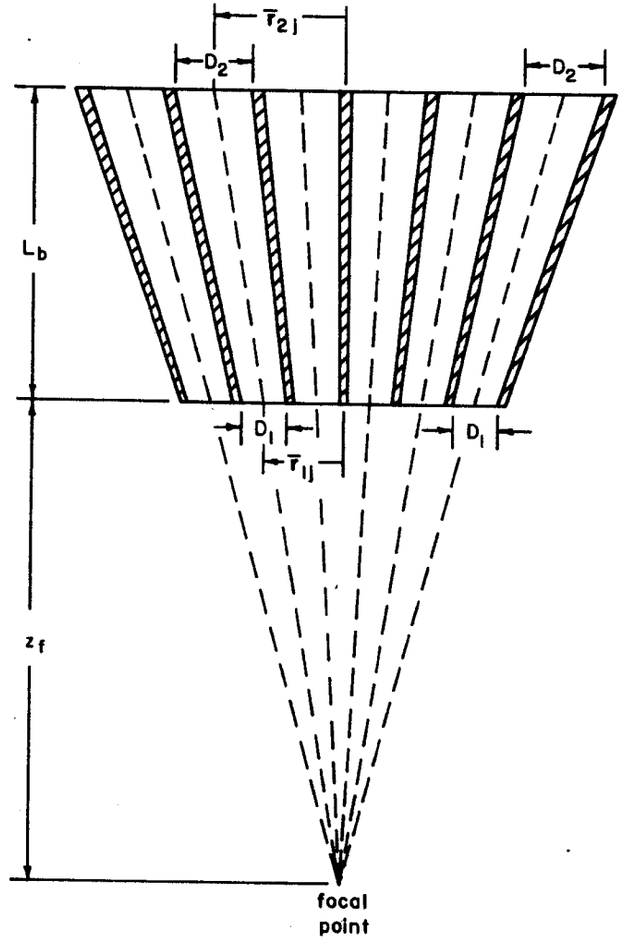

Fig. 4.21 Geometry of the focused collimator.

We need merely to generalize the single-bore results to allow for a nonconstant bore diameter and an overall tilt. As in the single-bore case, we can model each bore in a focused collimator by a pair of circular apertures. (In practice, the bores often have a hexagonal cross section, but little error occurs if we treat them as circular.) The lower aperture of the jth bore is described by

$$g_{1j}(\mathbf{r}') = \text{circ}(2|\mathbf{r}' - \bar{\mathbf{r}}_{1j}|/D_1), \tag{4.84}$$

while the upper aperture for the jth bore is given by

$$g_{2j}(\mathbf{r}'') = \text{circ}(2|\mathbf{r}'' - \bar{\mathbf{r}}_{2j}|/D_2). \tag{4.85}$$

Note that D_1 and D_2 are assumed to be the same for all bores.

If each bore is to point exactly to a common focal point at $z = z_f$ (a condition that is sometimes deliberately violated in practice), then we must have $\bar{\mathbf{r}}_{1j}$ parallel to $\bar{\mathbf{r}}_{2j}$, and their magnitudes must satisfy

$$\bar{r}_{2j}/\bar{r}_{1j} = (L_b + z_f)/z_f \qquad \text{for all} \quad j. \tag{4.86}$$

Usually the walls will also be tapered so that the aperture diameters are in the same proportions:

$$D_2/D_1 = (L_b + z_f)/z_f. \tag{4.87}$$

We can now write down a rather formidable expression for the PSF of the focused collimator by analogy with (4.75). The result is

$$p_{fc}(\mathbf{r}; z) = \frac{n_l \dot{C}}{v_s} \int_\infty d^2r'' \sum_{j=1}^{M_b} \text{circ}\left(\frac{2|\mathbf{r}'' - \bar{\mathbf{r}}_{2j}|}{D_2}\right) \text{circ}\left(\frac{2|a\mathbf{r}'' + b\mathbf{r} - \bar{\mathbf{r}}_{1j}|}{D_1}\right), \tag{4.88}$$

where a and b have the same meaning as before, and M_b is the number of bores in the collimator. The more masochistically inclined readers may proceed to Fourier-transform this equation and find the general expression for the MTF.

There is, however, one condition under which (4.88) can be considerably simplified, viz., $z = z_f$. This condition implies that the object being imaged lies entirely in the focal plane. Since we set up the problem so that all bore sights exactly overlap in the focal plane, we would expect the PSF in this case to be exactly proportional to the PSF of a single bore. To verify this conjecture, define

$$\mathbf{r}_j'' \equiv \mathbf{r}'' - \bar{\mathbf{r}}_{2j}. \tag{4.89}$$

Then, in the argument of the second circ function of (4.88), we have

$$\begin{aligned} a\mathbf{r}'' + b\mathbf{r} - \bar{\mathbf{r}}_{1j} &= a(\mathbf{r}_j'' + \bar{\mathbf{r}}_{2j}) + b\mathbf{r} - \bar{\mathbf{r}}_{1j} \\ &= a\mathbf{r}_j'' + b\mathbf{r}, \end{aligned} \tag{4.90}$$

where the last step follows from (4.86) and the fact that $a = z_f/(L_b + z_f)$ if $z = z_f$. Equation (4.88) now reads

$$p_{fc}(\mathbf{r}; z_f) = \frac{n_l \dot{C}}{v_s} \sum_{j=1}^{M_b} \int_\infty d^2r_j'' \, \text{circ}\left(\frac{2r_j''}{D_2}\right) \text{circ}\left(\frac{2|a\mathbf{r}_j'' + b\mathbf{r}|}{D_1}\right). \tag{4.91}$$

But each term in the sum is independent* of j and identical with the single-bore PSF given by (4.75) (except for the minor generalization of differing aperture diameters, $D_1 \neq D_2$). We have therefore shown, not surprisingly, that

$$p_{fc}(r; z_f) = M_b p_{sb}(r; z_f). \tag{4.92}$$

It should be noted that $p_{fc}(\mathbf{r}; z_f)$ exhibits no umbra region. By use of (4.87), (4.91) is seen to represent the *auto*correlation of a circ function rather than the cross correlation of two different circ functions.

4.4.6 Sensitivity and Resolution

An oft-used measure of sensitivity for a scanner is the planar sensitivity S. This parameter is defined as the count rate obtained when the scanner is viewing a uniform planar source of activity 1.0 μCi/cm^2. (See Appendix D for a discussion of radiation units.) In our notation, such a source is described by $f(\mathbf{r}) = \text{const}$. The value of the constant is fixed if we assume that each nuclear disintegration produces exactly one emitted gamma ray with an energy suitable for detection by the scanner. Then, since 1.0 μCi corresponds to 3.7×10^4 disintegrations/sec, we have

$$f(\mathbf{r}) = 3.7 \times 10^4 \quad \text{emitted photons/cm}^2\,\text{sec}, \tag{4.93}$$

Different isotopes will give different values for the numerical constant in this equation since, in general, the number of usable gamma rays per disintegration will be different from one.

The count rate is given in terms of the PSF by

$$\text{count rate} = (v_s/n_l) p_c(\mathbf{r}; z) ** f(\mathbf{r}), \tag{4.94}$$

where $p_c(\mathbf{r}; z)$ can refer to either $p_{sb}(\mathbf{r}; z)$ or $p_{fc}(\mathbf{r}; z)$. We shall consider the single-bore case first.

Since $f(\mathbf{r})$ is a constant, the convolution in (4.94) becomes a simple integral over the PSF. The planar sensitivity is then given by

$$S_{sb} = \frac{v_s}{n_l} (3.7 \times 10^4) \cdot \int_\infty p_{sb}(\mathbf{r}; z) \, d^2r \tag{4.95}$$

* The fact that $\mathbf{r}_j''$ depends on $\bar{\mathbf{r}}_{2j}$ is of no concern since $\mathbf{r}_j''$ is a dummy variable of integration, and the integration is over the entire $\mathbf{r}_j''$ = plane.

or, from (4.75) and (4.72),

$$S_{sb} = \frac{3.7 \times 10^4}{4\pi(L_b + z)^2} \int_\infty d^2r'' \int_\infty d^2r \,\mathrm{circ}\left(\frac{2r''}{D_b}\right)\mathrm{circ}\left(\frac{2|ar'' + br|}{D_b}\right). \quad (4.96)$$

where now L_b and z must be expressed in centimeters.

The integral over $\mathbf{r}$ in (4.96), which involves only the second circ function, is easily performed, with the result

$$S_{sb} = \frac{3.7 \times 10^4}{4\pi(L_b + z)^2} \frac{\pi D_b^2}{4b^2} \int_\infty d^2r'' \,\mathrm{circ}\left(\frac{2r''}{D_b}\right)$$
$$= \frac{3.7 \times 10^4}{4\pi(L_b + z)^2} \frac{\pi D_b^2}{4b^2} \frac{\pi D_b^2}{4}. \quad (4.97)$$

With the aid of the definition of b, (4.70), S_{sb} reduces further to

$$S_{sb} = \frac{3.7 \times 10^4}{64} \frac{\pi D_b^4}{L_b^2} \quad \frac{\text{counts/sec}}{\mu\text{Ci/cm}^2} \quad (4.98)$$

(all dimensions in centimeters). Note that this result is independent of z and the scan parameters v_s and n_1. It does not matter how far you are from a uniform source or how fast you are moving past it.

It is a simple matter to modify the preceding derivation so that it applies to a focused collimator. The result is

$$S_{fc} = \frac{3.7 \times 10^4}{64} M_b \frac{\pi D_1^2 D_2^2}{L_b^2} \quad \frac{\text{counts/sec}}{\mu\text{Ci/cm}^2} \quad (4.99)$$

(all dimensions in centimeters).

To put these expressions for sensitivity into proper perspective, it is useful to restate them in terms of the collimator's resolution distance defined, as usual, as the FWHM of the PSF. For the single-bore collimator, the resolution distance $\delta_{sb}(z)$ can be estimated from the approximate sketches given in Fig. 4.17, where the curvature of the PSF in the penumbra region is neglected. We find

$$\delta_{sb}(z) \approx D_b(1 + z/L_b). \quad (4.100)$$

Of course, if $z \to 0$, δ_{sb} will equal D_b without approximation.

If we regard D_b as the variable parameter and hold z and L_b fixed, we have

$$S_{sb} \propto \delta_{sb}^4. \quad (4.101)$$

Thus a twofold improvement in resolution (reduction in δ_{sb}) must come at the expense of a sixteenfold decrease in sensitivity. And even this drastic behavior understates the problem when noise is considered. Let us anticipate a simple result from Chapter 10, where it is shown that the signal-to-noise ratio (SNR) in a scanner image is determined by the number of detected photons *per resolution element*, which we shall denote by N_δ. For a given source, we have

$$N_\delta \propto S_{sb} \cdot \delta_{sb}^2 \propto \delta_{sb}^6. \quad (4.102)$$

To keep the SNR constant when δ_{sb} is reduced by a factor of 2, therefore, means that either the source activity or the total scan time must be increased by a factor of 64.

A somewhat different result applies to a focused collimator. In the focal plane the PSF, as noted previously, is proportional to the autocorrelation of a circ function. Numerical evaluation of this autocorrelation (Gaskill, 1978, p. 304) shows that the resolution distance is given by

$$\delta_{fc} = 0.808 D_1(1 + z_f/L_b). \quad (4.103)$$

(The factor of 0.808 would become unity if we neglected the curvature of the PSF.) Furthermore, since the ratio D_1/D_2 is fixed by (4.87), we have

$$S_{fc} \propto M_b D_1^4 \propto M_b \delta_{fc}^4, \quad (4.104)$$

for fixed z_f and L_b.

The major difference from the single-bore case arises when we realize that M_b itself is a function of D_1 or δ_{fc}. The reason is that the total diameter of the detector crystal is usually fixed. Therefore, if each bore is made smaller, more bores can be fit into the detector area. Specifically, we have

$$M_b = \alpha_{pf}(D_{det}/D_2)^2, \quad (4.105)$$

where D_{det} is the diameter of the detector and α_{pf} is the packing fraction, i.e., the fraction of the total area of the crystal that is covered by the open part of the collimator. If all bores point to a common focal point, α_{pf} is also the fraction of the detector area that can be seen from the focal point. For a given minimum septal thickness, α_{pf} will be the largest for a hexagonal array of bores. Typically, α_{pf} lies between 0.5 and 0.8, depending on septal thickness and hence on photon energy.

From (4.87), (4.103), and (4.105), we now have

$$M_b \propto \delta_{fc}^{-2} \quad (4.106)$$

where D_{det}, L_b, z_f, and α_{pf} are regarded as fixed. The number of counts per resolution element, in this case, is given by

$$N_\delta \propto S_{fc} \delta_{fc}^2 \propto \delta_{fc}^4. \quad (4.107)$$

In other words, a constant SNR can be maintained when halving δ_{fc} by "merely" increasing the source activity or the scan time a factor of 16. The

situation is still drastic, but at least it is an improvement over the single-bore case.

The fourth-power law given in (4.107) is quite common in radiographic imaging. For example, the reader may wish to test his understanding of the arguments in this section by showing that (4.107) applies also to pinhole imaging.

4.4.7 The Ratemeter

In this section we consider the contribution of the count-rate meter to the overall PSF of a scanner (Rao and Wagner, 1967; Beck, 1968a). One can imagine a scanner with very fine collimator bores so that the collimator PSF is vanishingly narrow. (Never mind that the photon collection efficiency is also vanishingly small—statistical considerations are not our concern at this stage. Since this is a gedankenexperiment, the source can be infinitely intense.) When this hypothetical collimator is raster-scanned over a point source, photons can be detected only when the collimator is positioned directly over the point. However, this is not to say that the image will be an ideal point. Instead the ratemeter will have a nonzero output, and hence the displayed image will be nonzero for some time after the collimator has passed the true location of the point. In fact, the PSF in the scan direction is just the temporal impulse response of the ratemeter with appropriate scale factors. When the collimator is directly over the source, a brief burst of photons is admitted to the detector which produces an equally brief electrical signal, approximating an impulse, as the input to the ratemeter. The electrical signal emerging from the ratemeter is then, by definition, its impulse response. Of course, this impulse response would normally be calculated as a function of time, but we can easily convert it to a function of position if we know the scan speed.

A corollary result is that the ratemeter cannot degrade the image at all in the direction perpendicular to the scan motion. To see this, note that if our hypothetical collimator is displaced slightly so that the scan line does not intersect the source point, no photons are ever admitted to the detector and no input signal is ever applied to the ratemeter. Hence, its output also remains zero.

To restate the conclusions of the last two paragraphs more formally, suppose that the scanner is moving in the x direction at a uniform speed v_s. Then the ratemeter contribution to the PSF is given by

$$p_{rm}(\mathbf{r}) = (1/v_s)\,\delta(y)\,q_{rm}(x/v_s), \tag{4.108}$$

where $q_{rm}(t)$ is the temporal impulse response of the ratemeter regarded as an electrical filter. The leading factor of $1/v_s$ in (4.108) is required so that

$p_{rm}(\mathbf{r})$ will have dimensions of inverse area. The temporal impulse response $q_{rm}(t)$ has dimensions of inverse time so that $(1/v_s)q(x/v_s)$ has dimensions of inverse length. Of course, $\delta(y)$ also has dimensions of inverse length. With this definition, $f(\mathbf{r}) ** p_{fc}(\mathbf{r}) ** p_{rm}(\mathbf{r})$ represents the number of detected photons per unit area [with $f(\mathbf{r})$, as usual, being the number of emitted photons per unit area per unit time].

As an example, we shall now calculate the PSF for the RC ratemeter depicted in Fig. 4.15. For simplicity, we assume that the output impedance of the amplifier driving the RC network is zero, while the input impedance of the following amplifier is infinite. The same current $i(t)$ thus flows through R_1 and C_1. From elementary circuit theory we then have

$$i(t) = C_1 \frac{dv_{out}(t)}{dt} \tag{4.109}$$

and

$$v_{in}(t) = i(t)R_1 + v_{out}(t). \tag{4.110}$$

Combining these equations, we find

$$R_1C_1 \frac{dv_{out}}{dt} + v_{out} = v_{in}. \tag{4.111}$$

The left-hand side of this equation may be rewritten, with the aid of the usual integrating factor,

$$R_1C_1 \exp\left(\frac{-t}{R_1C_1}\right)\frac{d}{dt}\left[v_{out}\exp\left(\frac{t}{R_1C_1}\right)\right] = v_{in}, \tag{4.112}$$

from which an integration and a little algebra yield

$$v_{out}(t) = \frac{1}{R_1C_1}\exp\left(\frac{-t}{R_1C_1}\right)\int_{-\infty}^{t} v_{in}(t')\exp\left(\frac{t'}{R_1C_1}\right)dt'. \tag{4.113}$$

Now what we are really interested in is not this general result so much as the special case where $v_{in}(t')$ is the unit impulse $\delta(t')$ and $v_{out}(t)$ is the impulse response $q_{rm}(t)$. The integration is then essentially trivial, but we must not forget that an integral involving a delta function can be nonzero only if the argument of the delta function vanishes within the domain of integration. We thus have

$$\begin{aligned} q_{rm}(t) &= \frac{1}{R_1C_1}\exp\left(\frac{-t}{R_1C_1}\right)\int_{-\infty}^{t}\delta(t')\exp\left(\frac{t'}{R_1C_1}\right)dt' \\ &= \begin{cases} (1/R_1C_1)\exp(-t/R_1C_1) & \text{if } t > 0 \\ 0 & \text{if } t < 0. \end{cases} \end{aligned} \tag{4.114}$$

The result that $q_{rm}(t) = 0$ if $t < 0$ should come as no surprise; it simply says that no output can be produced from an electrical filter before an input is applied. In this case the input is an impulse at $t = 0$.

The product R_1C_1 has dimensions of time and is called the *time constant* of the filter. Basically, the counts are averaged over this time before being displayed.

A compact notation for use in (4.114) is the Heaviside unit step function, defined by

$$\text{step}(t) = \begin{cases} 1 & \text{if } t > 0 \\ 0 & \text{if } t < 0. \end{cases} \tag{4.115}$$

In terms of this function, (4.114) becomes

$$q_{rm}(t) = \frac{1}{R_1C_1} \exp\left(\frac{-t}{R_1C_1}\right) \text{step}(t) \tag{4.116}$$

and, with (4.108), our final result for the ratemeter PSF is

$$p_{rm}(\mathbf{r}) = \frac{1}{v_s R_1 C_1} \exp\left(\frac{-x}{v_s R_1 C_1}\right) \delta(y)\,\text{step}(x). \tag{4.117}$$

The FWHM of this function is $v_s R_1 C_1 \ln 2$ in the x direction and, of course, zero in the y direction. It is plotted in Fig. 4.22.

To complete the analysis, we should now calculate the ratemeter contribution to the scanner transfer function. This can be accomplished either by directly transforming (4.117) or by returning to the circuit model and expressing the voltage transfer ratio in the temporal frequency (ν) domain. The latter approach yields

$$\frac{V_{out}(\nu)}{V_{in}(\nu)} = \frac{(2\pi i \nu C_1)^{-1}}{R_1 + (2\pi i \nu C_1)^{-1}} = \frac{1}{1 + 2\pi i \nu R_1 C_1}, \tag{4.118}$$

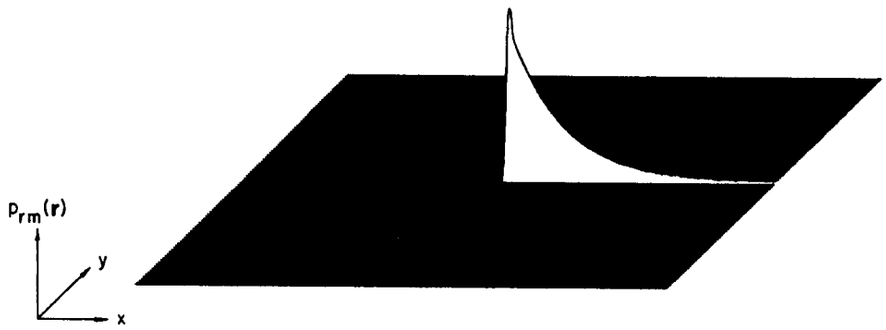

Fig. 4.22 Isometric plot of the ratemeter contribution to the scanner PSF.

where $V_{out}(\nu)$ and $V_{in}(\nu)$ are the temporal Fourier transforms of $v_{out}(t)$ and $v_{in}(t)$, respectively, and $i = \sqrt{-1}$ [not to be confused with the current $i(t)$]. The temporal frequency ν is related to ξ, the x component of the spatial frequency, by

$$\nu = \xi v_s. \tag{4.119}$$

The spatial transfer function is thus

$$TF_{rm}(\boldsymbol{\rho}) = P_{rm}(\boldsymbol{\rho}) = [1 + 2\pi i \xi v_s R_1 C_1]^{-1}. \tag{4.120}$$

Note that this function is independent of η, the y component of $\boldsymbol{\rho}$, since the ratemeter cannot degrade the image in the y direction.

Equation (4.120) is interesting because $P_{rm}(\boldsymbol{\rho})$ is a complex function. To interpret this result, it is helpful to rewrite it in modulus-phase form:

$$P_{rm}(\boldsymbol{\rho}) = [1 + (2\pi\xi v_s R_1 C_1)^2]^{-1/2} \exp(i\phi_{rm}), \tag{4.121}$$

where

$$\phi_{rm} = -\tan^{-1}(2\pi\xi v_s R_1 C_1). \tag{4.122}$$

In other words, if a sinusoidal activity pattern with spatial frequency ξ were to be scanned with our hypothetical ideal collimator and with a ratemeter time constant of R_1C_1, the contrast of the displayed image would be reduced by a factor of $[1 + (2\pi\xi v_s R_1 C_1)^2]^{-1/2}$ and the phase of the pattern would be shifted by ϕ_{rm}. The MTF, $|P_{rm}(\boldsymbol{\rho})/P_{rm}(0)|$, is plotted in Fig. 4.23.

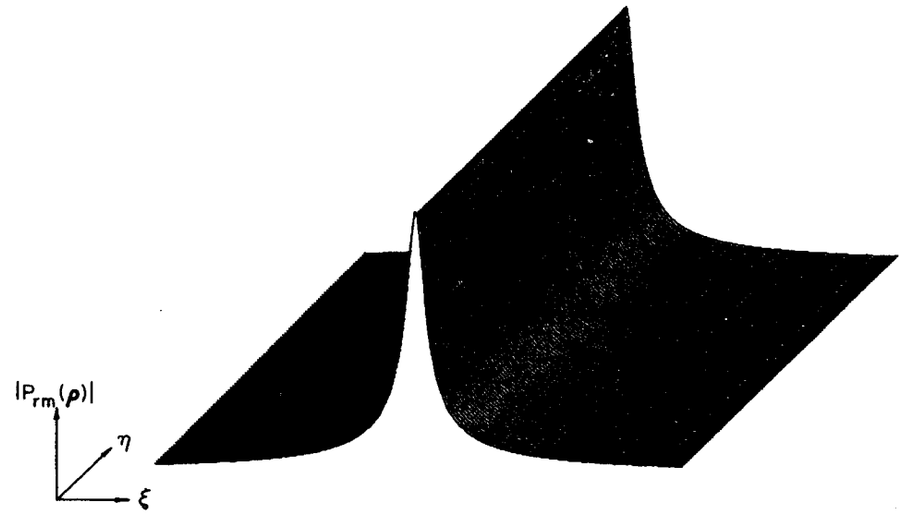

Fig. 4.23 Isometric plot of the ratemeter contribution to the scanner MTF. The origin ($\xi = 0, \eta = 0$) is at the center of the figure.

4.4.8 Image Display and Overall System Characterization

The most common way to display the image from a scintillation scanner is to use a modulated light source moving in synchronism with the scanner head to expose a piece of film. If the light intensity is modulated in proportion to the output of the ratemeter, then the film exposure is a linear function of the gamma-ray activity in the source, and the techniques of linear systems theory may be used to describe the film-exposing device. Of course, the film itself responds nonlinearly to the exposure, but this creates no real difficulty since the film characteristics are presumably known. The optical density of the developed film is thus easily calculated from the exposure, which in turn is calculated by successively convolving the gamma-ray source distribution $f(\mathbf{r})$ with the PSF's describing the collimator, the ratemeter, and the display.

There is one subtlety in this prescription. A convolution integral cannot be a rigorous description of the action of a scanner since the scanner detector does not systematically explore all possible points on the x–y plane as implied by a continuous integral. Rather the detector is usually swept continuously in the x direction but moved in discrete steps in the y direction. However the film exposure, which we shall call $E(x, y)$, is defined over the entire film plane (although it may be zero for some x–y values). The display spread function evidently enters our formalism somewhat differently than the collimator and ratemeter PSFs.

To pursue this point, let us lump the collimator and ratemeter PSFs into a single function $p_{\text{crm}}(\mathbf{r})$ defined by

$$p_{\text{crm}}(\mathbf{r}) = p_{\text{c}}(\mathbf{r}) ** p_{\text{rm}}(\mathbf{r}), \tag{4.123}$$

where $p_{\text{c}}(\mathbf{r})$ may be either $p_{\text{fc}}(\mathbf{r})$ or $p_{\text{sb}}(\mathbf{r})$ as appropriate. We adopt the viewpoint that the scanner head is stationary and the source moves continuously along a sequence of lines described by $y = y_k$, with k being an integer index. The interval between scan lines is n_l^{-1} where n_l, as previously defined, is the number of scan lines per unit length. The voltage output from the ratemeter, when the instantaneous shift of the source relative to the detector is (x_0, y_k), is given by an ordinary convolution:

$$v_{\text{out}}(x_0, y_k) \propto \int_{-\infty}^{\infty}\int_{-\infty}^{\infty} dx'\,dy'\, p_{\text{crm}}(x', y') f(x_0 - x', y_k - y'). \tag{4.124}$$

Let us suppose that the light source illuminates a square aperture of side ε_{a} that is imaged at unit magnification onto the film. (Note that if $\varepsilon_{\text{a}} = n_l^{-1}$, the exposed scan lines will be contiguous.) Then, for the particular

relative shift (x_0, y_k), the film exposure pattern is described by

$$E_{x_0 y_k}(x, y) \propto v_{\text{out}}(x_0, y_k)\,\text{rect}\left(\frac{x - x_0}{\varepsilon_{\text{a}}}\right)\text{rect}\left(\frac{y - y_k}{\varepsilon_{\text{a}}}\right). \tag{4.125}$$

The total film exposure $E(x, y)$ is obtained by summing (4.125) over all possible source-detector shifts; the sum becomes an integral over the continuous variable x_0 but remains a discrete sum over y_k. The result is

$$E(x, y) \propto \sum_k \int_{-\infty}^{\infty} dx_0\,\text{rect}\left(\frac{x - x_0}{\varepsilon_{\text{a}}}\right)\text{rect}\left(\frac{y - y_k}{\varepsilon_{\text{a}}}\right) \cdot \int_{-\infty}^{\infty}\int_{-\infty}^{\infty} dx'\,dy'\, p_{\text{crm}}(x', y') f(x_0 - x', y_k - y'). \tag{4.126}$$

This equation looks very much like a repeated convolution except that *one* of the integrals has been replaced by a sum. But this is a nontrivial change. To see that (4.126) is not even approximately a continuous convolution, one has only to consider the limit $\varepsilon_{\text{a}} \to 0$. Then the film is exposed only along thin lines and is unexposed between lines. This is, of course, a very poor display format but, more important for the present discussion, it is one that cannot be obtained by convolving $f(x, y)$ with any realistic function. Instead, the proper description of (4.126) follows the lines of the sampling theory discussion given in Section 2.5; the scanner *samples* the image in the y direction.

It was shown in Section 2.5 that a band-limited function can be recovered from its samples by a low-pass filtering operation if the Nyquist condition, (2.82), is satisfied. For the present problem the function being sampled is $p_{\text{crm}}(\mathbf{r}) ** f(\mathbf{r})$, and the sampling rate $1/\Delta$ is just n_l. Let us assume that the collimator MTF is essentially zero for all y-directed spatial frequencies greater than $\eta_{\max}$. (The ratemeter MTF does not enter this discussion since it influences only the x-directed spatial frequencies.) Then the Nyquist condition is $n_l > 2\eta_{\max}$. No assumptions about $f(\mathbf{r})$ are needed.

The required low-pass filter may be an implicit rather than explicit part of the system. A physician viewing a scanner image will often unconsciously adjust his viewing distance so that his eye cannot resolve the scan lines. Or, even if he can see them, he has learned to ignore the scan lines and concentrate on the underlying image structure. The low-pass filter is thus the observer's eye or brain.

In any event, if n_l is large enough, it is safe to say that we are interested in only the low-frequency components of $E(x, y)$, which we shall denote by $E_{\text{lf}}(x, y)$. The derivation of $E_{\text{lf}}(x, y)$ parallels the derivation of (2.87). As far

as the y dependence is concerned, (4.126) has the form [cf. (2.69)]

$$\begin{aligned} E(x, y) &\propto \sum_k s(y_k)\,\mathrm{rect}\left(\frac{y - y_k}{\varepsilon_a}\right) \\ &= \left[\sum_k s(y_k)\,\delta(y - y_k)\right] * \mathrm{rect}\left(\frac{y}{\varepsilon_a}\right) \\ &= \left[s(y)\sum_k \delta(y - y_k)\right] * \mathrm{rect}\left(\frac{y}{\varepsilon_a}\right), \end{aligned} \tag{4.127}$$

where

$$\begin{aligned} s(y_k) \equiv \int_{-\infty}^{\infty} dx_0\,\mathrm{rect}\left(\frac{x - x_0}{\varepsilon_a}\right) \\ \times \int_{-\infty}^{\infty}\int_{-\infty}^{\infty} p_{\mathrm{crm}}(x', y') f(x_0 - x', y_k - y')\,dx'\,dy'. \end{aligned} \tag{4.128}$$

Since the y_k values are evenly spaced, we can write $y_k = k/n_l$ and hence

$$\begin{aligned} \sum_k \delta(y - y_k) &= \sum_k \delta\left[y - \left(\frac{k}{n_l}\right)\right] \\ &= n_l \sum_k \delta(n_l y - k) = n_l\,\mathrm{comb}(n_l y). \end{aligned} \tag{4.129}$$

A one-dimensional Fourier transform on $E(x, y)$ then yields

$$\begin{aligned} \mathscr{F}_y\{E(x, y)\} &\propto [S(\eta) * \mathrm{comb}(\eta/n_l)]\,\mathrm{sinc}(\varepsilon_a \eta) \\ &= \left[n_l \sum_k S(\eta - k n_l)\right]\mathrm{sinc}(\varepsilon_a \eta). \end{aligned} \tag{4.130}$$

The low-pass filter serves to select the $k = 0$ term in this sum and reject all others. An inverse transform then gives

$$E_{\mathrm{lf}}(x, y) \propto s(y) * \mathrm{rect}(y/\varepsilon_a). \tag{4.131}$$

Combining (4.131) and (4.128) and rewriting them in convolution form, we now have

$$E_{\mathrm{lf}}(x, y) \propto \left[\mathrm{rect}\left(\frac{x}{\varepsilon_a}\right)\mathrm{rect}\left(\frac{y}{\varepsilon_a}\right)\right] ** p_{\mathrm{crm}}(x, y) ** f(x, y), \tag{4.132}$$

which we might have written down intuitively at the outset. In other words, if we consider only the low-frequency components, it *is* rigorously correct to ascribe a PSF to the film-exposing device even though (4.126) could not be written in convolution form.

Furthermore, the display PSF need not be simply the square aperture considered thus far. It can readily be modified to any positive-definite function simply by inserting appropriate transparencies in the optical system. The film exposure system is thus a convenient place to control the overall PSF of a scanner (Tsui *et al.*, 1980). Of course, only smoothing and not sharpening operations are possible in the display since we are restricted to positive-definite PSFs. Still, it might be preferable to smooth the data with the display rather than with the ratemeter since the former provides a two-dimensional averaging, while the latter affects only the scan direction.

4.5 COLLIMATORS FOR SCINTILLATION CAMERAS

Fundamentally, collimators for use with scintillation cameras are no different from those used with scanners (Causer, 1974; Rotenberg and Johns, 1965; Miracle *et al.*, 1979). The typical parallel-hole camera collimator can be viewed either as an array of identical single-bore collimators as described in Sections 4.4.2 and 4.4.3, or equivalently as the focused collimator of Section 4.4.5 in the limit where the focal distance z_f approaches infinity. A magnifying camera collimator is nothing but a focused scanner collimator with z_f much greater than the actual object distance z (although in practice the camera collimator will have many more holes). Similarly, a minifying camera collimator is a focused scanner collimator where z_f is large and negative.

Nevertheless, the present section is not superfluous; we cannot simply rewrite the expression for the PSF of a scanner collimator and claim to have solved the corresponding problem for a camera. Nontrivial differences arise because a camera measures the x–y coordinates of each gamma ray that interacts with the scintillation crystal, while a scanner simply counts them.

In one sense the camera case is simpler because one less integration is involved. For the scanner we had to first calculate the x–y distribution of incident photons on the crystal face and then integrate it to get the total count rate. By simply deleting the last integration we should have the desired x–y distribution for a camera. This is indeed correct, but unfortunately, not very useful, because the PSF so determined is not shift-invariant. As illustrated in Fig. 4.24, the shape of the image of a point depends on the location of the point relative to the collimator. This is a serious problem because it means that the response to an arbitrary input cannot be written as a convolution, and a simple transfer function cannot be defined.

An ingenious artifice to avoid this difficulty, introduced by Hal Anger, is the "average PSF" obtained by averaging a point-source image over all possible source locations. This approach is detailed in Section 4.5.1 and given a more rigorous justification based on sampling theory in Section 4.5.2.

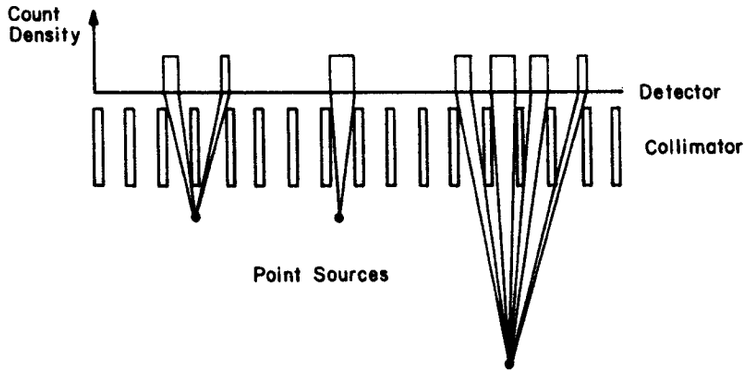

Fig. 4.24 Illustration of shift-variant imaging with a parallel-hole collimator.

The upshot of this discussion is that a shift-invariant PSF can indeed be defined and we can proceed in an orderly way to calculate the transfer function and to consider practical design tradeoffs.

4.5.1 The Average PSF

A problem that sometimes arises when a high-energy low-resolution collimator (one with large bores and thick septa) is used is that the shadows of the septa can be seen on the final image. Since this regular geometrical pattern can be annoying and may interfere with the diagnostic process, Wilks *et al.* (1969) constructed a device called a "collywobbler" to wobble the collimator back and forth during the exposure, blurring out the septal shadows. Since there was no relative movement of the object and the detector, the collywobbler did not substantially affect the image resolution.

The collywobbler was a mechanical realization of an earlier suggestion by Anger (1964) who calculated the PSF of a collimator by assuming that it was moving even if, in fact, it was not. Since moving the collimator alone is equivalent to moving the source and detector in synchronism while keeping the collimator fixed, Anger's "mathematical collywobbler" calculation gave the average shape of the PSF, averaged over all possible locations of the source point. Thus, even though the Wilks collywobbler is not often used in practice, it is nevertheless a useful conceptual device.

The substance of the Anger calculation can be seen by modeling each bore of a parallel-hole collimator as a pair of circular apertures, just as we did in Section 4.4.3. For simplicity we assume for now that the image detector is exactly coplanar with the upper aperture; this restriction will be lifted in Section 4.5.3. We consider a unit point source located at the point $\mathbf{r}_s$ and denote the resulting point spread function by $p_{\text{phc}}(\mathbf{r}'';\mathbf{r}_s)$. Two separate arguments $\mathbf{r}''$ and $\mathbf{r}_s$ are required since the function is not shift invariant;

location in both the image plane and the source plane must be specified. In general, $p_{\text{phc}}(\mathbf{r}'';\mathbf{r}_s)$ will also depend on the z coordinate of the source point, but this dependence has been suppressed here in order to keep the notation from becoming any more unwieldy.

The function $p_{\text{phc}}(\mathbf{r}'';\mathbf{r}_s)$ can be obtained from $p_{sb}(\mathbf{r}_s;z)$ as given by (4.75) by four simple modifications:

(1) The integration over $\mathbf{r}''$ must be deleted since we are dealing with an imaging rather than an integrating detector.

(2) The factor of n_l/v_s, peculiar to the scanner, must be deleted and the exposure time T must be reinserted.

(3) Each circ function must be displaced by an amount $\bar{\mathbf{r}}_k$, where the kth bore in the collimator is centered at $\mathbf{r} = \bar{\mathbf{r}}_k$.

(4) A sum over all bores must be performed.

The result is

$$p_{\text{phc}}(\mathbf{r}'';\mathbf{r}_s) = C\sum_k \text{circ}\left[\frac{2|\mathbf{r}''-\bar{\mathbf{r}}_k|}{D_b}\right]\text{circ}\left[\frac{2|a\mathbf{r}''+b\mathbf{r}_s-\bar{\mathbf{r}}_k|}{D_b}\right], \quad (4.133)$$

where a and b still have the meanings given by (4.70).

We now want to average this expression over all possible positions of the collimator, with the source point $\mathbf{r}_s$ and the observation point $\mathbf{r}''$ held fixed. To shift the collimator, we simply add a vector $\mathbf{R}$ to each $\bar{\mathbf{r}}_k$ in (4.133). The average PSF, averaged over a disk of radius R_m, is then given by

$$\langle p_{\text{phc}}(\mathbf{r}'';\mathbf{r}_s)\rangle_{R_m} = \frac{C}{\pi R_m^2}\int_{\text{disc}} d^2R \sum_k \text{circ}\left[\frac{2|\mathbf{r}''-\bar{\mathbf{r}}_k-\mathbf{R}|}{D_b}\right] \times \text{circ}\left[\frac{2|a\mathbf{r}''+b\mathbf{r}_s-\bar{\mathbf{r}}_k-\mathbf{R}|}{D_b}\right]. \quad (4.134)$$

Now if we ignore the collimator boundaries and allow R_m to approach infinity, each term in the sum over k gives the same value for the integral. The number of such terms, i.e., the number of bores in the area πR_m^2, is given by

$$K = \alpha_{\text{pf}}(2R_m/D_b)^2, \quad (4.135)$$

where α_{pf} is the packing fraction defined just as in the scanner case. Then, since $K/\pi R_m^2 = 4\alpha_{\text{pf}}/\pi D_b^2$, we have

$$\langle p_{\text{phc}}(\mathbf{r}'';\mathbf{r}_s)\rangle_{R_m} = \frac{4\alpha_{\text{pf}}}{\pi D_b^2} C\int_\infty d^2R\,\text{circ}\left[\frac{2|\mathbf{r}''-\mathbf{R}|}{D_b}\right] \times \text{circ}\left[\frac{2|a\mathbf{r}''+b\mathbf{r}_s-\mathbf{R}|}{D_b}\right]. \quad (4.136)$$

Note that R_m no longer appears in this result.

Equation (4.136) can be simplified somewhat by a change of variables,

$$\mathbf{R}' = \mathbf{R} - \mathbf{r}'', \tag{4.137}$$

which gives

$$\langle p_{\text{phc}}(\mathbf{r}'';\mathbf{r}_s)\rangle_{R_m} = \frac{4\alpha_{\text{pf}}}{\pi D_b^2} C \int_\infty d^2R' \,\text{circ}\left[\frac{2R'}{D_b}\right] \times \text{circ}\left[\frac{2|(a-1)\mathbf{r}'' + b\mathbf{r}_s - \mathbf{R}'|}{D_b}\right]. \tag{4.138}$$

But, from (4.70), $a + b = 1$, so that

$$(a-1)\mathbf{r}'' + b\mathbf{r}_s = b(\mathbf{r}_s - \mathbf{r}''). \tag{4.139}$$

With this substitution, (4.138) takes the form of the autoconvolution of a circ function (which is the same as the autocorrelation since the circ is an even function) evaluated at a "shift" of $b(\mathbf{r}_s - \mathbf{r}'')$, i.e.,

$$\langle p_{\text{phc}}(\mathbf{r}'';\mathbf{r}_s)\rangle_{R_m} = \frac{4\alpha_{\text{pf}}}{\pi D_b^2} C \,[g_1(\mathbf{r}) ** g_1(\mathbf{r})]_{\mathbf{r}=b(\mathbf{r}_s-\mathbf{r}'')}, \tag{4.140}$$

where, as before, $g_1(\mathbf{r})$ denotes circ $(2r/D_b)$. Equation (4.140) can be generalized to apply to a collimator with parallel but tapered bores by replacing $g_1(\mathbf{r}) ** g_1(\mathbf{r})$ by $g_2(\mathbf{r}) ** g_1(\mathbf{r})$, where g_1 and g_2 denote circ functions of diameter D_1 and D_2, respectively.

We have now shown explicitly that $\mathbf{r}_s$ and $\mathbf{r}''$ enter into $\langle p_{\text{phc}}(\mathbf{r}'';\mathbf{r}_s)\rangle$ only in the shift-invariant combination $\mathbf{r}_s - \mathbf{r}''$. We are thus justified in simplifying our notation and bringing it into line with that of previous sections by writing

$$\langle p_{\text{phc}}(\mathbf{r}'';\mathbf{r}_s)\rangle_{R_m} = \bar{p}_{\text{phc}}(\mathbf{r}'' - \mathbf{r}_s) = \bar{p}_{\text{phc}}(\mathbf{r}), \tag{4.141}$$

where $\mathbf{r} = \mathbf{r}'' - \mathbf{r}_s$. Because the magnification of the parallel-hole collimator is $+1$, this simple change of variables is sufficient to go from the point *image* in the $\mathbf{r}''$ plane, $\bar{p}_{\text{phc}}(\mathbf{r}'' - \mathbf{r}_s)$, to the *point spread function* in the $\mathbf{r}$ plane. The overbar is retained as a remainder that we are dealing with an average PSF.

Compare $\bar{p}_{\text{phc}}(\mathbf{r})$, which is plotted in Fig. 4.25 with $p_{\text{sb}}(\mathbf{r})$ shown in Fig. 4.20. The latter function is not an autocorrelation, but rather the correlation of two different circ functions of different scales. It therefore has a flat top that we referred to as the umbra region. By contrast, $\bar{p}_{\text{phc}}(\mathbf{r})$ is precisely an autocorrelation and exhibits no umbra. This difference may appear strange at first since the integrand in (4.136) for $\bar{p}_{\text{phc}}(\mathbf{r})$ is so similar to that in (4.75) for $p_{\text{sb}}(\mathbf{r})$. To understand the difference, it is important to look at just what is being calculated. For $p_{\text{sb}}(\mathbf{r})$ the integration is over $\mathbf{r}''$; viewed as functions of

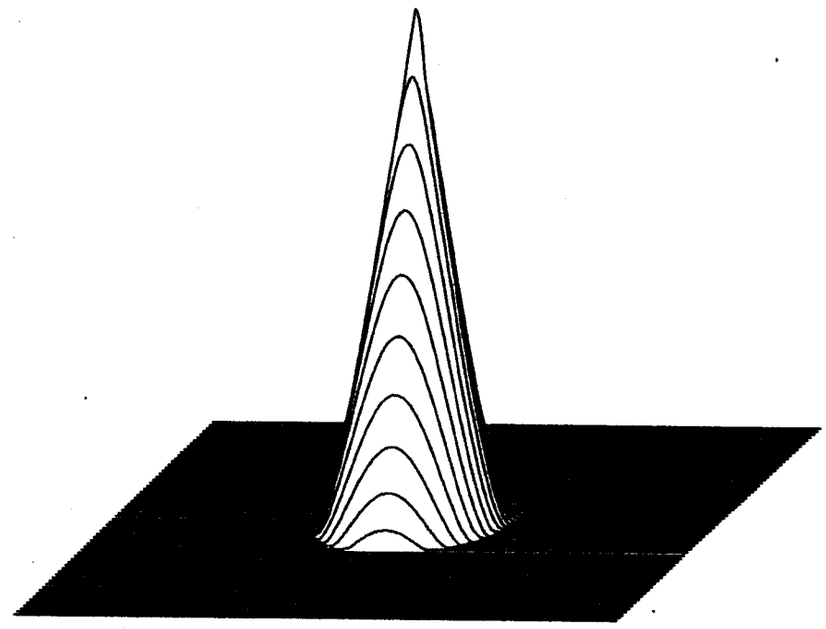

Fig. 4.25 Average PSF for a parallel-hole collimator. This function is the autocorrelation of a circ function.

$\mathbf{r}''$ the two circ functions have different scales. For $\bar{p}_{\text{phc}}(\mathbf{r})$ on the other hand, the integral is over the shift parameter $\mathbf{R}$; as functions of $\mathbf{R}$ the two circ functions of (4.136) have the *same* scale.

4.5.2 Sampling Theory Analysis

Let us back up to the stage of (4.133) in Section 4.5.1 where we had a general expression for the shift-variant PSF before any averaging had been applied. If, at this stage, the sum over k had been replaced with an integral over $\bar{\mathbf{r}}_k$, we could easily have written $p_{\text{phc}}(\mathbf{r}'';\mathbf{r}_s)$ as a convolution and, in fact, would have obtained (4.140), our final expression for $\bar{p}_{\text{phc}}(\mathbf{r})$. In other words, the averaging process is equivalent to replacing the sum in (4.133) by an integral.

We have encountered this same situation once before. In discussing the image-display portion of a scanner, we found that the film exposure, given by (4.126), had the form of a convolution except that one of the integrals had been replaced by a sum. In that case, we found that the difference between sum and integral disappeared if the sampling rate was adequate and we considered only the low-frequency components of the image. We shall now show that the same conclusion follows for the present problem.

Because of the various shifts and scale factors involved, this problem gets rather tedious in the space domain. A more orderly approach is to immediately transform (4.133) and carry out most of the manipulations in the frequency domain. To this end, let us rewrite (4.133)

$$p_{\text{phc}}(\mathbf{r}'';\mathbf{r}_s) = C\sum_k g_1(\mathbf{r}''-\bar{\mathbf{r}}_k)\tilde{g}_1\left(\mathbf{r}''+\frac{b}{a}\mathbf{r}_s-\frac{1}{a}\bar{\mathbf{r}}_k\right), \tag{4.142}$$

where $\tilde{g}_1(\mathbf{r})$ is the scaled circ function defined previously [see (4.73) and (4.78)]. We now compute the Fourier transform of this equation *with respect to the* $\mathbf{r}''$ *variable only*; $\mathbf{r}_s$ is treated as a fixed parameter. Physically, this is equivalent to fixing the location of a source point at $\mathbf{r}=\mathbf{r}_s$, forming an image, and then performing a two-dimensional transform on the image. By use of the shift theorem of Fourier theory, (B.95), we have

$$\begin{aligned} P_{\text{phc}}(\boldsymbol{\rho}'';\mathbf{r}_s) &\equiv \mathscr{F}_2\{p_{\text{phc}}(\mathbf{r}'';\mathbf{r}_s)\} \\ &= C\sum_k [\exp(-2\pi i\boldsymbol{\rho}''\cdot\bar{\mathbf{r}}_k)G_1(\boldsymbol{\rho}'')] \\ &\quad ** \left\{\exp\left[-2\pi i\boldsymbol{\rho}''\cdot\left(\frac{1}{a}\mathbf{r}_k-\frac{b}{a}\mathbf{r}_s\right)\right]\tilde{G}_1(\boldsymbol{\rho}'')\right\}. \end{aligned} \tag{4.143}$$

Writing out the convolution integral in this equation in detail, we find

$$\begin{aligned} P_{\text{phc}}(\boldsymbol{\rho}'';\mathbf{r}_s) &= C\sum_k \int_\infty d^2\rho' \exp(-2\pi i\boldsymbol{\rho}'\cdot\bar{\mathbf{r}}_k)G_1(\boldsymbol{\rho}') \\ &\quad \times \exp\left[-2\pi i(\boldsymbol{\rho}''-\boldsymbol{\rho}')\cdot\left(\frac{1}{a}\bar{\mathbf{r}}_k-\frac{b}{a}\mathbf{r}_s\right)\right]\tilde{G}_1(\boldsymbol{\rho}''-\boldsymbol{\rho}'). \end{aligned} \tag{4.144}$$

Collecting together all terms involving $\bar{\mathbf{r}}_k$, we recognize that they are the Fourier transform of a sum of delta functions:

$$\begin{aligned} \sum_k \exp\left[-2\pi i\bar{\mathbf{r}}_k\cdot\left(\boldsymbol{\rho}'+\frac{1}{a}(\boldsymbol{\rho}''-\boldsymbol{\rho}')\right)\right] &= \int_\infty d^2r \exp(-2\pi i\mathbf{r}\cdot\boldsymbol{\rho})\sum_k \delta(\mathbf{r}-\bar{\mathbf{r}}_k) \\ &= \mathscr{F}_2\left\{\sum_k[\delta(\mathbf{r}-\bar{\mathbf{r}}_k)]\right\} \end{aligned} \tag{4.145}$$

where

$$\boldsymbol{\rho} = \boldsymbol{\rho}' + (1/a)(\boldsymbol{\rho}''-\boldsymbol{\rho}'). \tag{4.146}$$

Now if the bore centers $\bar{\mathbf{r}}_k$ form a square array with spacing ε_b, the sum of delta functions is just a two-dimensional comb function:

$$\sum_k \delta(\mathbf{r}-\bar{\mathbf{r}}_k) = \frac{1}{\varepsilon_b^2}\operatorname{comb}\left(\frac{\mathbf{r}}{\varepsilon_b}\right). \tag{4.147}$$

We are treating the array here as infinite even though real collimators are finite. This is a small error if the number of bores in the collimator is large.

The Fourier transform of this comb function is also a comb [see (B.48)],

$$\mathscr{F}_2\left\{\sum_k \delta(\mathbf{r}-\bar{\mathbf{r}}_k)\right\} = \operatorname{comb}(\varepsilon_b\boldsymbol{\rho}) = \frac{1}{\varepsilon_b^2}\sum_k \delta(\boldsymbol{\rho}-\boldsymbol{\rho}_k), \tag{4.148}$$

where the $\boldsymbol{\rho}_k$ vectors also form a square array, but with spacing $1/\varepsilon_b$.

Equation (4.144) now becomes

$$\begin{aligned} P_{\text{phc}}(\boldsymbol{\rho}'';\mathbf{r}_s) &= \frac{C}{\varepsilon_b^2}\sum_k \int_\infty d^2\rho' \exp\left(2\pi i(\boldsymbol{\rho}''-\boldsymbol{\rho}')\frac{b}{a}\mathbf{r}_s\right) \\ &\quad \times \delta(\boldsymbol{\rho}-\boldsymbol{\rho}_k)G_1(\boldsymbol{\rho}')\tilde{G}_1(\boldsymbol{\rho}''-\boldsymbol{\rho}'). \end{aligned} \tag{4.149}$$

The delta function in this equation can be rewritten, using (4.146),

$$\delta(\boldsymbol{\rho}-\boldsymbol{\rho}_k) = \delta[\boldsymbol{\rho}' + (1/a)(\boldsymbol{\rho}''-\boldsymbol{\rho}') - \boldsymbol{\rho}_k] \tag{4.150}$$

or, since $a = 1-b$,

$$\begin{aligned} \delta(\boldsymbol{\rho}-\boldsymbol{\rho}_k) &= \delta[\boldsymbol{\rho}'(1-1/a) + (1/a)\boldsymbol{\rho}'' - \boldsymbol{\rho}_k] \\ &= (a^2/b^2)\delta[\boldsymbol{\rho}' + (a/b)\boldsymbol{\rho}_k - (1/b)\boldsymbol{\rho}'']. \end{aligned} \tag{4.151}$$

We thus find, after some algebra,

$$\begin{aligned} P_{\text{phc}}(\boldsymbol{\rho}'';\mathbf{r}_s) &= \frac{C}{\varepsilon_b^2}\frac{a^2}{b^2}\sum_k \exp[2\pi i(\boldsymbol{\rho}_k-\boldsymbol{\rho}'')\cdot\mathbf{r}_s] \\ &\quad \times G_1\left(-\frac{a}{b}\boldsymbol{\rho}_k+\frac{1}{b}\boldsymbol{\rho}''\right)\tilde{G}_1\left(\frac{a}{b}\boldsymbol{\rho}_k-\frac{a}{b}\boldsymbol{\rho}''\right). \end{aligned} \tag{4.152}$$

If ε_b is small enough, a condition to be defined more precisely below, then the various terms in this sum will not overlap significantly and a low-pass filter (which could be the scintillation camera detector itself) may be used to isolate the single term for which $\boldsymbol{\rho}_k = 0$. In the frequency domain, this filtered image may be written

$$[P_{\text{phc}}(\boldsymbol{\rho}'';\mathbf{r}_s)]_{\text{lf}} = \frac{a^2}{b^2}\frac{C}{\varepsilon_b^2}\exp(-2\pi i\boldsymbol{\rho}''\cdot\mathbf{r}_s)G_1\left(\frac{\boldsymbol{\rho}''}{b}\right)\tilde{G}_1\left(\frac{-a\boldsymbol{\rho}''}{b}\right). \tag{4.153}$$

But, since $g_1(\mathbf{r}')$ is real and symmetric,

$$\tilde{G}_1(-a\boldsymbol{\rho}''/b) = \tilde{G}_1(a\boldsymbol{\rho}''/b) = (1/a^2)G(\boldsymbol{\rho}''/b).$$

An inverse transform thus yields

$$[p_{\text{phc}}(\mathbf{r}'';\mathbf{r}_s)]_{\text{lf}} = \frac{C}{\varepsilon_b^2}[g_1(\mathbf{r}') ** g_1(\mathbf{r}')]_{\mathbf{r}'=b(\mathbf{r}''-\mathbf{r}_s)}. \tag{4.154}$$

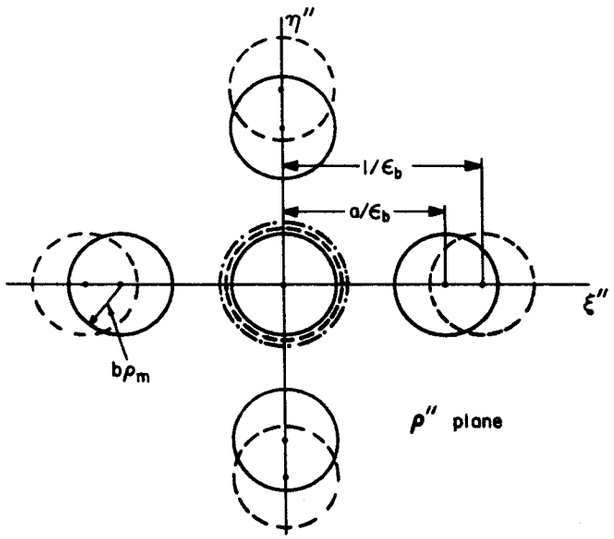

Fig. 4.26 Location of the various terms of Eq. (4.152) in the ρ'' plane. Solid circles: regions of support for $G_1[-(a\rho_k/b)+(\rho''/b)]$; dashed circles: regions of support for $\tilde{G}_1[(a\rho_k/b)-(a\rho''/b)]$; dot-dashed circle: passband of low-pass filter.

This result is in full accord with (4.140) since $\alpha_{pf}\varepsilon_b^2 = \pi D_b^2/4$. Low-pass filtering is thus equivalent to "collywobbler averaging".

An essential step in this derivation was the use of a low-pass filter to isolate a single term in (4.152). We now inquire under what condition this is possible. We need to consider only the zero-order term ($\rho_k = 0$) and the four surrounding first-order terms, all of which have $|\rho_k| = 1/\varepsilon_b$. If none of the first-order terms overlap the zero-order terms, then none of the higher-order terms will either. The location and extent of the various orders is indicated in Fig. 4.26. In constructing this diagram the center of each region was first found by setting the argument of the corresponding function to zero, since $G_1(\rho'')$ is a maximum for $\rho''=0$. For example, $G_1[-(a\rho_k/b)+(\rho''/b)]$ in (4.152) has orders centered on the ξ'' axis at $\xi'' = \pm a/\varepsilon_b$ (where ξ'' and η'' are the Cartesian components of ρ''). The diameter of the circular region is found by asserting that $G_1(\rho)$ has significant values only if ρ is less than some maximum value which we shall denote by ρ_m. From this it follows that $G_1(\rho''/b)$ is significant only within a circle of radius $b\rho_m$ in the ρ'' plane. Similar arguments for the orders lying along the η'' axis and for the $\tilde{G}_1$ factors in (4.152) then lead to the complete diagram of Fig. 4.26.

From the diagram it is seen that there is no overlap of orders if

$$a\rho_k \geq 2b\rho_m. \tag{4.155}$$

This condition will insure that the kth-order G_1 terms will not overlap either zero-order term. The condition for no overlap of the kth-order $\tilde{G}_1$ terms and the zero order is $\rho_k > 2b\rho_m$, but since $a < 1$, (4.155) is the more stringent condition.

If (4.155) is satisfied for the lowest-order term, $\rho_k = 1/\varepsilon_b$, it will be satisfied for all orders. Therefore, using the definition of a and b from (4.70), we require

$$z/\varepsilon_b \geq 2L_b\rho_m. \tag{4.156}$$

As a rough estimate, we may take $\rho_m = 1/D_b$. Furthermore, if the septa are thin, $D_b \approx \varepsilon_b$. The results of this section are thus valid if

$$z \gtrsim 2L_b. \tag{4.157}$$

In clinical practice, z will usually be at least $2L_b$ since L_b is typically only 2–3 cm. We are thus justified in using the shift-invariant PSF, (4.154) or (4.140), to describe a camera collimator.

4.5.3 Modulation Transfer Function

Before writing down an expression for the modulation transfer function (MTF), we shall first generalize the PSF to allow for the possibility of a gap between the exit face of the collimator and the detector crystal. This is a simple modification because the photons continue to travel in straight lines as they traverse the gap. For a point source, the radiation pattern incident on the crystal is just a magnified version of the pattern emerging from the collimator. The magnification factor, by analogy with projection radiography, is

$$m_g = \frac{L_g + L_b + z}{L_b + z}, \tag{4.158}$$

where L_g is the gap length. The magnified point image is obtained from (4.140) by the substitution of $\mathbf{r}''/m_g$ for $\mathbf{r}''$ in the argument of $p_{phc}(\mathbf{r}'')$, with a suitable amplitude scaling to conserve photons. The modified expression for the average PSF is thus

$$\bar{p}_{phc}(\mathbf{r}'') = \frac{4\alpha_{pf}}{\pi D_b^2}\frac{C}{m_g^2}\left[g_1(\mathbf{r}') ** g_1(\mathbf{r}')\right]_{\mathbf{r}'=b\mathbf{r}''/m_g}. \tag{4.159}$$

The leading factor of C/m_g^2 has a simple interpretation since

$$\frac{C}{m_g^2} = \frac{T}{4\pi(L_b+z)^2}\left(\frac{L_b+z}{L_b+z+L_g}\right)^2 = \frac{T}{4\pi(L_b+z+L_g)^2}. \tag{4.160}$$

In other words, since the distance from source to detector has been increased

from $L_b + z$ to $L_b + z + L_g$, the appropriate distance to use in the inverse-square law is now $L_b + z + L_g$.

Even though the point image is magnified when the gap is present, the magnification of the *collimator* is still $+1$. In other words, two points a distance x apart in the $\mathbf{r}$ plane still produce two point images with a center-to-center spacing of x in the $\mathbf{r}''$ plane. The point-spread function is just $\bar{p}_{phc}(\mathbf{r})$, obtained from (4.159) by letting $\mathbf{r}'' \to \mathbf{r}$.

The Fourier transform of $\bar{p}_{phc}(\mathbf{r})$ is now easily performed. By use of the scaling law, (B.94), we find

$$\bar{P}_{phc}(\rho) = \frac{4\alpha_{pf}}{\pi D_b^2}\frac{C}{b^2}\left[G_1\left(\frac{m_g\rho}{b}\right)\right]^2. \tag{4.161}$$

Since $g_1(\mathbf{r})$ is the circ function of diameter D_b, we know from (B.114) that

$$G_1(\rho) = \frac{\pi D_b^2}{4}\frac{2J_1(\pi D_b\rho)}{\pi D_b\rho}. \tag{4.162}$$

The average MTF for the parallel-hole camera collimator is thus

$$\overline{\mathrm{MTF}}_{phc}(\rho) \equiv \left|\frac{\bar{P}_{phc}(\rho)}{\bar{P}_{phc}(0)}\right| = \left|\frac{2J_1(\pi m_g D_b\rho/b)}{\pi m_g D_b\rho/b}\right|^2. \tag{4.163}$$

It is worth noting that $\bar{P}_{phc}(\rho)$ is everywhere real and positive. The problem of phase shifts in the transfer function discussed earlier does not occur here, and the MTF is a complete description of the system.

4.5.4 Resolution and Collection Efficiency

Having obtained an expression for the PSF, we may now readily compute the collimator resolution distance defined as usual as the FWHM of the PSF.

Since, by (4.159), the average collimator PSF is the autocorrelation of a circ function, we need to determine what shift is required between two identical circ functions to reduce their overlap area to one-half the area of either function separately. By numerically evaluating the autocorrelation, we find that the required shift is $0.808R$, where R is the radius of the circ function.

However, we note from (4.159) that the autocorrelation in $\bar{p}_{phc}$ is calculated with the shift variable given by $b\mathbf{r}''/m_g$. To find the resolution distance δ_{phc}, we must set $r'' = \delta_{phc}/2$ and then demand that the shift be equal to $0.808D_b/2$. In other words,

$$b\delta_{phc}/2m_g = 0.808D_b/2, \tag{4.164}$$

or, using the definition of b from (4.70) and of m_g from (4.158), we have

$$\delta_{phc} = 0.808D_b\frac{L_g + L_b + z}{L_b}. \tag{4.165}$$

Several conclusions can be immediately drawn from this result. The first is that a gap between the collimator and detector (nonzero L_g) is bad. The detector should always be as close to the exit surface of the collimator as practical. Another important conclusion is that a parallel-hole collimator has its best resolution (smallest δ_{phc}) when the object is closest to the entrance face of the collimator (small z).

Finally, (4.165) shows that the collimator resolution is always improved by making the length of the bores, L_b, greater. We should not conclude from this, however, that a very large L_b is always desirable. The difficulty is that L_b also influences the collection efficiency of the collimator. This point is most easily seen by considering a point source in contact with the entrance face of the collimator (and not hidden by the septa). The fractional solid angle for photon collection is then given by

$$[\Omega/4\pi]_{z=0} = D_b^2/16L_b^2, \tag{4.166}$$

which obviously falls off rapidly if L_b is increased.

It is a little trickier to calculate the dependence of $\Omega/4\pi$ on L_b if $z \neq 0$ since in that case more than one collimator bore can collect photons from each object point. In fact, the graphical construction of Fig. 4.27 shows that the number of participating bores is given approximately by $\alpha_{pf}(L_b + z)^2/L_b^2$. Then, since the distance from the point source to the exit face of the collimator

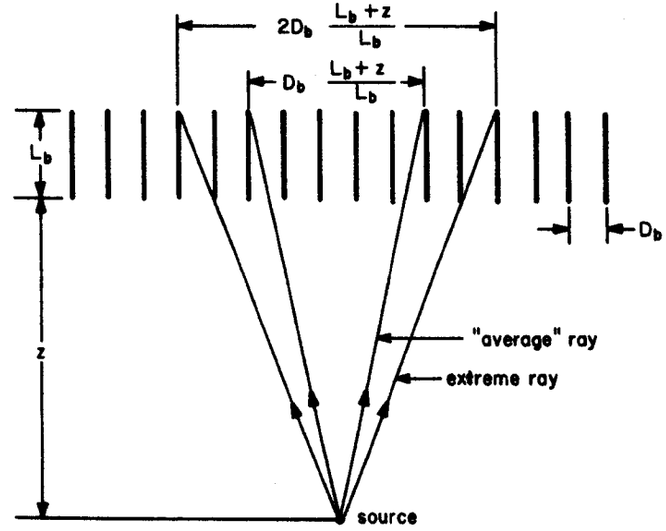

Fig. 4.27 Diagram for the calculation of collection efficiency of a parallel-hole collimator when $z \neq 0$.

is $L_b + z$, the fractional solid angle subtended by all bores is [cf. (4.166)]

$$\frac{\Omega}{4\pi} = \frac{D_b^2}{16(L_b + z)^2} \frac{\alpha_{pf}(L_b + z)^2}{L_b^2} = \frac{\alpha_{pf} D_b^2}{16 L_b^2}. \tag{4.167}$$

In other words, if the septa are thin so that the packing fraction is near 1, the efficiency of a parallel-hole collimator is nearly independent of the source location and equal to the value for $z = 0$ given in (4.166).

The graphical arguments that led to (4.167) will now be replaced by a more rigorous analytical treatment. The key point to recognize is that the area integral of the PSF represents the mean number of counts collected from a unit point source. Since a unit point source is, by definition, one which on the average emits one photon per unit time, the integral of the PSF must be identical to $\Omega T/4\pi$. The calculation of the collection efficiency of a parallel-hole collimator thus reduces to the problem of integrating the autocorrelation of a circ function. [See (4.59).]

This integral might seem to be fairly difficult, but the central ordinate theorem of Fourier theory, (B.96), comes to our rescue. For any function $f(\mathbf{r})$ we have

$$\int_\infty f(\mathbf{r})\, d^2r = [\mathscr{F}_2\{f(\mathbf{r})\}]_{\rho=0} = F(0). \tag{4.168}$$

Therefore, letting $f(\mathbf{r})$ be $g_1(\mathbf{r}) ** g_1(\mathbf{r})$, we find

$$\int_\infty [g_1(\mathbf{r}) ** g_1(\mathbf{r})]\, d^2r = [G_1(0)]^2. \tag{4.169}$$

But $G_1(0)$ may itself be determined by the central ordinate theorem:

$$G_1(0) = \int_\infty g_1(\mathbf{r})\, d^2r = \frac{\pi D_b^2}{4}. \tag{4.170}$$

We now apply these results, together with the scaling theorem (B.94) to the expression for $\bar{p}_{phc}$ given in (4.159). The result is

$$\frac{\Omega T}{4\pi} = \int_\infty \bar{p}_{phc}(\mathbf{r}'')\, d^2r'' = \frac{4\alpha_{pf}}{\pi D_b^2} \frac{C}{m_g^2} \left(\frac{m_g}{b}\right)^2 \left(\frac{\pi D_b^2}{4}\right)^2. \tag{4.171}$$

By use of the definitions of b and C from (4.70) and (4.72), respectively, we again arrive at (4.167). Note that m_g cancels out of $\Omega/4\pi$, as it must since the collection efficiency has already been determined once the photons emerge from the collimator; no photons are lost in traversing the gap.

Equation (4.167) for the efficiency and (4.165) for the resolution distance are the basic design equations for parallel-hole camera collimators. The trade-offs involved are illustrated in Fig. 4.28 where we plot δ_{phc} and $\Omega/4\pi$ for three hypothetical collimators. We see from this figure that the source

Collimator No.	Bore Diameter D_b	Bore Length L_b
1	2.5 mm	20 mm
2	2.5 mm	10 mm
3	5 mm	20 mm

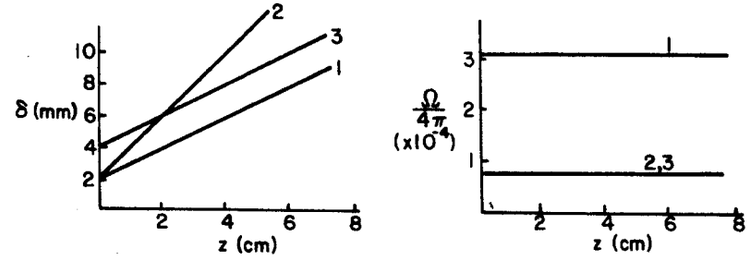

Fig. 4.28 Variation of resolution and efficiency with z for three hypothetical parallel-hole collimators.

distance z is an important consideration in collimator design. If we could place the collimator in contact with the source ($z = 0$), an obvious impossibility for sources within the body, then we could obtain any desired resolution without loss of efficiency simply by decreasing D_b and L_b in the same proportion. The drawback of this approach is that the choice of a small L_b leads to a collimator whose performance degrades rapidly as z is increased.

4.5.5 Comparison of the Parallel-Hole Collimator and the Pinhole

An important practical question that often arises is whether to use a pinhole or a collimator in a particular situation. This simple question turns out to be surprisingly slippery. As in any comparison, we must first state what is being held constant, what is being varied, and what is being compared. To limit the choices somewhat, let us rather arbitrarily fix the resolution and the field of view and compare collection efficiencies. For the parallel-hole collimator, the field of view is just equal to the detector diameter d''_{det}. The same FOV is obtained for the pinhole if $s_1 = s_2$ so that the magnification is unity [see (4.45)]. This choice has the additional virtue that detector resolution limitations affect the pinhole and collimator cameras in the same way since the magnifications are equal.

We now set $\delta_{ph} = \delta_{phc}$ and use (4.35) and (4.165) to eliminate d'_{ph} and D_b. Equations (4.33) and (4.167) may then be combined to yield

$$\frac{\Omega_{phc}}{\Omega_{ph}} = \frac{4\alpha_{pf} s_1^2}{(0.808)^2 (L_g + L_b + z)^2}. \tag{4.172}$$

In this equation s_1 refers to the pinhole geometry while L_g, L_b, and z refer to the parallel-hole collimator. In practice, s_1 is limited by obliquity considerations as discussed in Section 4.2.6. However, if we ignore that problem for the moment, the best performance with both systems is obtained by putting the pinhole or the collimator as close to the source as possible, for example in contact with the patient's skin, thus making $s_1 = z$. By plugging in typical numbers for $\alpha_{pf}(\sim 0.5\text{–}0.8)$, $L_g(\sim 2\text{–}3$ cm), $L_b(\sim 2\text{–}6$ cm), and $z(\sim 2\text{–}15$ cm), we see that the collimator usually has a modest advantage in collection efficiency over a pinhole. However, the large variability in the parameters precludes dogmatism.

Two limits are of some interest. If $z \gg L_g + L_b$ and $\alpha_{pf} \approx (0.808)^2$, we find that the collimator has a fourfold advantage. The opposite extreme of $L_g + L_b \gg z$ would seem to greatly favor the pinhole, but in fact this is not so, at least in medical applications. For such small z values the obliquity considerations for the pinhole, which were ignored in the formulation of (4.172), strongly reduce both the efficiency and the FOV of the pinhole camera. In practice, a pinhole will seldom if ever have an efficiency advantage over a parallel-hole collimator. The usefulness of the pinhole lies in the ease with which magnification can be changed, allowing the region of interest effectively to fill the available detector area.

An important similarity between pinhole and collimator imaging comes up when we contemplate decreasing the resolution distance of either system. If we improve the resolution of the pinhole by decreasing d'_{ph} while holding s_1 and s_2 fixed, (4.33) and (4.35) show that $\Omega_{ph} \propto d'^2_{ph} \propto \delta^2_{ph}$. Similarly, we may improve the resolution of the collimator by holding L_g, L_b, and z fixed and decreasing D_b. Then (4.165) and (4.167) show that $\Omega_{phc} \propto D_b^2 \propto \delta^2_{phc}$. Reducing the resolution distance thus requires a compensating increase in either patient dose or exposure time. In fact, by arguments similar to those adduced for scanners in Section 4.4.6, we can show (and shall do so in Chapter X) that the required dose or exposure time for constant signal-to-noise ratio varies inversely as the fourth power of the resolution distance [cf. (4.107)]. In other words, a twofold improvement in the resolution of the collimator or pinhole must be accompanied by a 16-fold increase in either the exposure time or the amount of radioactivity in the object if we wish to maintain constant SNR.

Precisely this same result was shown in Section 4.4.6 to apply to a scanner used with a multibore focused collimator. However, the result has even more serious implications for pinhole or collimator imaging with a scintillation camera because the resolution distance referred to in the fourth-power law is the one appropriate to the pinhole or collimator *alone*. There is a further image degradation, not present in a scanner, due to the image detector. Thus

even if we do reduce D_b or d'_{ph} by a factor of 2, the overall system resolution is improved by a smaller factor. The lesson to be drawn is that it is extraordinarily difficult to improve resolution in nuclear imaging.

4.5.6 Detector Considerations: Minifying and Magnifying Collimators

Although it was mentioned in Section 4.5.5, the image detector has not yet been included in our formulation. For a parallel-hole collimator, inclusion of the detector is trivial since the collimator has a magnification of unity. As in Section 4.2.5, we describe the detector either by a transfer function $D(\rho)$ or by a PSF, $d(\mathbf{r})$. The unit magnification eliminates the need for any scaling factors and we have directly

$$p_{det}(\mathbf{r}) = d(\mathbf{r}) \tag{4.173}$$

and

$$p_{tot}(\mathbf{r}) = p_{phc}(\mathbf{r}) ** p_{det}(\mathbf{r}). \tag{4.174}$$

One conclusion to be drawn from this equation is that the final image resolution with a parallel-hole collimator can never be better than the resolution of the detector itself. Since the intrinsic resolution distance of typical scintillation detectors such as the Anger camera is usually about 4–8 mm, magnification techniques that enlarge the image onto the detector face are highly desirable. We have already discussed this approach in connection with pinhole imaging in Section 4.2.5. However, we also showed in Section 4.5.5 that pinholes are usually somewhat less efficient than collimators, especially when obliquity factors are taken into account. These considerations have led in recent years to the development of magnifying collimators as depicted in Fig. 1.22.

Conversely, there are some clinical applications where resolution is relatively unimportant but a large field of view is required. For these cases a minifying collimator as shown in Fig. 1.21 can be used. It is worth noting that a minifying collimator is an upside-down magnifying collimator, a fact that can be used to reduce the number of collimators a department must acquire.

In this section we shall not make any great distinction between a magnifying and a minifying collimator. Mathematically they are virtually indistinguishable and we shall use the subscript mc for both.

We assume that all bores in the collimator point to a common focal point a distance z_f from the entrance face of the collimator; z_f is a positive number for a magnifying collimator and a negative one for a minifying

collimator. In either case, the magnification is given by

$$m_{mc} = \frac{z_f + L_b + L_g}{z_f - z}, \tag{4.175}$$

where $m_{mc} > 1$ for a magnifying collimator and $m_{mc} < 1$ for a minifying one. (Note that z, L_b, and L_g are always *positive* numbers.) If $z_f \to \pm\infty$, we are back to the parallel-hole case and $m_{mc} \to 1$. Note also that very large magnifications can be obtained by setting $z \approx z_f$. However large minification ratios are more difficult since they require $z \gg |z_f|$.

The next step is to modify our previous results for collimator PSF, resolution, and efficiency so that they will apply to magnifying and minifying collimators. It is not so obvious that this step is possible since we have relied so heavily on the average-PSF concept introduced in Section 4.5.1. With a magnifying or minifying collimator we cannot form a reasonable average PSF by holding the source and detector fixed and translating the collimator over all possible positions since this corresponds to moving the image spot all over the detector. The resulting PSF would be huge and meaningless. Collywobblers do not work with magnifying or minifying collimators.

A closely related trick can, however, be employed. Suppose we hold the collimator fixed, move the source point through a vector distance $\mathbf{R}$, and move the detector by $m_{mc}\mathbf{R}$. Then the center of the image of the point remains stationary relative to the detector and integration over all $\mathbf{R}$ yields a very reasonable average PSF. Of course, this is purely a mathematical device, not a practical way to remove collimator structure.

The remainder of the calculation closely parallels Section 4.5.1. We start with (4.88) for the PSF of a focused scanner collimator and modify it by deleting the integral over $\mathbf{r}''$ and replacing the factor of n_l/v_s with T. This leaves

$$p_{mc}(\mathbf{r}''; \mathbf{r}_s) = C \sum_j \operatorname{circ}\left(\frac{2|\mathbf{r}'' - \bar{\mathbf{r}}_{2j}|}{D_2}\right) \operatorname{circ}\left[\frac{2|a\mathbf{r}'' + b\mathbf{r}_s - \bar{\mathbf{r}}_{1j}|}{D_1}\right], \tag{4.176}$$

where, as in Section 4.4.5, $\bar{\mathbf{r}}_{1j}$ and $\bar{\mathbf{r}}_{2j}$ denote the center positions of the lower and upper apertures of the jth bore, and D_1 and D_2 are their diameters. Equations (4.86) and (4.87) are also assumed to still hold.

The averaging process described above may be written out explicitly by substituting $(\mathbf{r}'' - m_{mc}\mathbf{R})$ for $\mathbf{r}''$ and $(\mathbf{r}_s - \mathbf{R})$ for $\mathbf{r}_s$ in (4.176), and then integrating over $\mathbf{R}$. The result is [cf. (4.134)]

$$\langle p_{mc}(\mathbf{r}''; \mathbf{r}_s)\rangle_{R_m} = \frac{C}{\pi R_m^2} \int_{\text{disc}} d^2R \sum_j \operatorname{circ}\left[\frac{2|\mathbf{r}'' - \bar{\mathbf{r}}_{2j} - m_{mc}\mathbf{R}|}{D_2}\right] \times \operatorname{circ}\left[\frac{2|a(\mathbf{r}'' - m_{mc}\mathbf{R}) + b(\mathbf{r}_s - \mathbf{R}) - \bar{\mathbf{r}}_{1j}|}{D_1}\right], \tag{4.177}$$

where the integral is over a disk of radius R_m, and we have assumed that the collimator-detector gap L_g is zero, a restriction that can be lifted later. If $R_m \to \infty$, all terms in the sum lead to the same value for the integral. To calculate the number of such terms, note that when the vector $\mathbf{R}$ explores all points within the disk of radius R_m, the center of the first circ function in (4.177) sweeps out an area in the $\mathbf{r}''$ plane given by $\pi(m_{mc}R_m)^2$. The number of terms in the sum, K, is then just the number of bores of diameter D_2 that will fit in this area. Thus [cf. (4.135)],

$$K = \alpha_{pf}(2m_{mc}R_m/D_2)^2 \tag{4.178}$$

and

$$K/\pi R_m^2 = (4\alpha_{pf}/\pi D_2^2)m_{mc}^2. \tag{4.179}$$

The following change of variables in (4.177) is now useful:

$$\mathbf{R}' = m_{mc}\mathbf{R} - \mathbf{r}'' - \bar{\mathbf{r}}_{2j}. \tag{4.180}$$

Note that this change also requires a modification of the area element since $d^2R = (m_{mc})^{-2}\, d^2R'$. We can now use (4.86), (4.87), (4.175), and (4.179), plus a fair amount of algebra, to rewrite (4.177)

$$\begin{aligned}\langle p_{mc}(\mathbf{r}''; \mathbf{r}_s)\rangle &= C\frac{4\alpha_{pf}}{\pi D_2^2}\int_\infty d^2R' \operatorname{circ}\left(\frac{2R'}{D_2}\right)\operatorname{circ}\left[\frac{2}{D_2}\left|b\frac{D_2}{D_1}\left(\mathbf{r}_s - \frac{\mathbf{r}''}{m_{mc}}\right) - \mathbf{R}'\right|\right] \\ &= C\frac{4\alpha_{pf}}{\pi D_2^2}\left[g_2(\mathbf{r}') ** g_2(\mathbf{r}')\right]_{\mathbf{r}' = b(D_2/D_1)(\mathbf{r}_s - \mathbf{r}''/m_{mc})},\end{aligned} \tag{4.181}$$

where

$$g_2(\mathbf{r}') = \operatorname{circ}(2r'/D_2). \tag{4.182}$$

All that remains is to refer this average PSF back to the original object scale and to recast our notation in a form that is more evidently shift invariant. We can combine these steps by defining

$$\begin{aligned}\bar{p}_{mc}(\mathbf{r} - \mathbf{r}_s) &\equiv m_{mc}^2\langle p_{mc}(m_{mc}\mathbf{r}; \mathbf{r}_s)\rangle \\ &= C\frac{4\alpha_{pf}}{\pi D_2^2} m_{mc}^2\left[g_2(\mathbf{r}') ** g_2(\mathbf{r}')\right]_{\mathbf{r}' = b(D_2/D_1)(\mathbf{r}_s - \mathbf{r})}.\end{aligned} \tag{4.183}$$

There is virtually no difference between the functional form of this equation and that of the corresponding equation for the parallel-hole case, (4.140). The factor of D_2/D_1 in the shift variable is of minor import since, by (4.87), $D_2 \approx D_1 \approx D_b$ if $z_f \gg L_b$, a condition that is certainly satisfied for any practical collimator. The conclusion is that a magnifying or minifying collimator has essentially the same PSF and resolution as a parallel-hole

collimator with the same values of the parameters L_b, D_b, and z. Similarly, it should not require an elaborate calculation to convince the reader that the results of Section 4.5.3, where a collimator-detector gap was allowed and the transfer function was calculated, are still applicable.

On the other hand, it is worthwhile to reconsider the results of Section 4.5.4 for the collection efficiency. Equation (4.183) differs from its counterpart, (4.140), in one important respect—the leading factor of m_{mc}^2. Therefore, by retracing the analysis that led up to the efficiency expression for the parallel-hole case, (4.167), we find that the efficiency of a magnifying or minifying collimator is

$$\frac{\Omega}{4\pi} = \frac{D_b^2 m_{mc}^2}{16 L_b^2} \alpha_{pf}. \tag{4.184}$$

In other words, a magnifying collimator becomes *more* efficient as the source is moved away from the collimator face while a minifying collimator becomes *less* efficient.

To conclude this section, we shall state the result for the composite PSF of a system consisting of a scintillation detector and either a magnifying or minifying collimator. The result is

$$p_{tot}(\mathbf{r}) = p_{det}(\mathbf{r}) ** p_{mc}(\mathbf{r}), \tag{4.185}$$

where

$$p_{det}(\mathbf{r}) = m_{mc}^2 d(m_{mc}\mathbf{r}). \tag{4.186}$$

The proof of this result follows the lines of Section 4.2.5 [cf. (4.44)].

The importance of (4.186) is that by use of a magnifying collimator ($m_{mc} > 1$) we can make $p_{det}(\mathbf{r})$ effectively narrower and reduce the image degradation due to the detector. Of course, the price must be paid in field of view.

4.6 FURTHER COMPLICATIONS

A linear, shift-invariant system is a mythical beast. The analyses given so far in this chapter must fail, to a greater or lesser degree, when applied to real radiographic systems which can be neither exactly linear nor exactly shift invariant. The purpose of this section is to catalog the factors that cause the breakdown of our simple models and to comment briefly on some of them.

The factors neglected so far include:

1. scattered radiation;
2. statistical fluctuations;

3. shift-variant imaging due to:
   a. the obliquity ($\cos^3\theta$) factor;
   b. nonparallelism of source and detector planes;
   c. anisotropic emission;
4. septal penetration;
5. patient motion;
6. problems associated with three-dimensional objects;
7. spectral effects;
8. detector limitations, including
   a. quantum efficiency;
   b. nonlinearities;
   c. geometrical distortions.

The first two items on this list, scattered radiation and statistical fluctuations, are enormously important in the analysis of radiographic systems. A separate chapter is devoted to each later in this book. Detector limitations are discussed in some detail for specific detectors in Chapter 5. Spectral effects are discussed in Chapters 7 and 11. The remaining topics are treated in this section.

4.6.1 Shift Variance

Real imaging systems are always shift-variant if for no other reason than their finite size; a point whose image entirely misses the detector cannot produce the same response as one in the center of the field of view. Several other, more subtle, sources of shift-variant behavior were mentioned and then ignored in the development of the general model in Section 4.1.

One justification for ignoring these effects is that, with the exception of the detector-boundary problem, they vary slowly with the position of the object point. Astronomers are fond of talking about an "isoplanatic patch," by which they mean an ill-defined (but scarcely nebulous) patch of sky over which the shape of a star image is "essentially constant." The source of the shift variance in astronomy—atmospheric inhomogeneities—is absent in radiographic imaging, but the principle is still applicable.

Before treating specific sources of shift variance, a brief comment on notation is required. We have already used two slightly different notations to denote the point response of an imaging system. For a general shift-variant system the response measured at point $\mathbf{r}$ due to an object at $\mathbf{r}_0$ was denoted by $p(\mathbf{r};\mathbf{r}_0)$. For a shift-invariant system the response function was written $p(\mathbf{r} - \mathbf{r}_0)$. For application of the isoplanatic patch concept, still a

third notation is useful. We acknowledge that the response depends strongly on the difference $\mathbf{r} - \mathbf{r}_0$ and only weakly on the absolute object position $\mathbf{r}_0$ by writing it $p[\mathbf{r} - \mathbf{r}_0, \mathbf{r}_0]$. To avoid confusion with $p(\mathbf{r}; \mathbf{r}_0)$, we shall use square brackets instead of parentheses and a comma instead of a semicolon in this new notation.

Of the systems discussed so far, shift variance is the least troublesome for the scintillation scanner. In this case only the boundary of the raster pattern causes any significant deviation from the true shift invariance. If we agree not to consider points within, say, twice the FWHM of the PSF of the edge of the field of view, then it is an excellent approximation to ignore the shift-variant behavior.

Shift variance may also be ignored, at least insofar as the image-forming operation is concerned, with a camera-collimator combination. Away from the boundary, the collimator may be treated as shift-invariant if we interpret the PSF in terms of either the "collywobbler-average" function of Section 4.5.1 or the filtered image of Section 4.5.2. Of course, the camera *detector* can respond differently to different source points even though the *collimator* is shift-invariant. Typically an Anger camera has poorer resolution at the edge of the field of view, shows some degree of geometric distortion, and has a sensitivity that varies by perhaps $\pm 10\%$ over the field. The source of these difficulties is discussed in Chapter 5.

Pinhole cameras are only slightly more complicated in this regard. The $\cos^3\theta$ factor reduces the amplitude of the PSF as the edge of the field is approached, but the shape of the PSF is virtually unchanged over the field if the aperture plate is thin. (Recall that a circular pinhole projected from any angle produces a circular image if the detector plane is parallel to the aperture plane.) A thick aperture plate does result in a shape change for large θ, as indicated in Fig. 4.9, but this effect can be minimized by tapering the pinhole. In other words, the shift-variant point response for a pinhole can, to a good approximation, be factored as

$$p_{\text{ph}}[\mathbf{r} - \mathbf{r}_0, \mathbf{r}_0] = \cos^3\theta(\mathbf{r}_0) p_{\text{ph}}(\mathbf{r} - \mathbf{r}_0), \tag{4.187}$$

where $p_{\text{ph}}(\mathbf{r} - \mathbf{r}_0)$ was calculated in Section 4.2.

The case in which shift variance is most important is transmission radiography. Practical x-ray tubes almost always have a tilted anode, as shown in Fig. 1.6, in order to reduce the projected area of the focal spot.

To analyze the tilted-anode geometry and to simultaneously allow for the fact that bremsstrahlung emission is far from isotropic, we introduce the concept of *photon radiance*, denoted by $L(\mathbf{r}_s, \hat{\mathbf{n}}_0)$, where $\mathbf{r}_s$ is a *three-dimensional* vector specifying position on the source and $\hat{\mathbf{n}}_0$ is a three-dimensional unit vector pointing from the source point to the object point of interest. The photon radiance is defined such that $L(\mathbf{r}_s, \hat{\mathbf{n}}_0)\, da_s\, d\Omega$ is the number of photons per second emitted by a source element of area da_s into the solid angle $d\Omega$ in the direction $\hat{\mathbf{n}}_0$. This definition differs from the usual definition of radiance in optics in two respects. First, it is expressed in terms of photon flux density per steradian rather than energy flux density per steradian. These two quantities are related by the photon energy. The second difference is more subtle. In optics, the area involved in the definition of radiance is usually taken as the *projected* area of the source projected onto a plane normal to the direction of propagation. With this definition, diffuse optical radiators (Lambertian surfaces) have constant radiance, independent of orientation. There is no analog of diffuse radiators in radiology, so a definition in terms of actual source area rather than projected area is more natural.

Suppose that the x-ray anode is a plane tilted at an angle θ_a measured from the z axis as shown in Fig. 4.29. The vector $\mathbf{r}_s$ is confined to this plane. The normal to the plane is defined by a unit vector $\hat{\mathbf{n}}_s$ given by

$$\hat{\mathbf{n}}_s = (0, \cos\theta_a, \sin\theta_a). \tag{4.188}$$

Therefore,

$$\mathbf{r}_s \cdot \hat{\mathbf{n}}_s = 0. \tag{4.189}$$

To make contact with our previous theory, we must project the photon radiance onto the x–y plane and thereby determine the emission function $f(\mathbf{r})$ defined in Section 4.1.1. Here, $\mathbf{r}$ is a two-dimensional vector in the x–y plane, or, equivalently, a three-dimensional vector whose z component is zero. The photons which are emitted from point $\mathbf{r}_s$ in the direction of $\hat{\mathbf{n}}_0$ will pass through the x–y plane at point $\mathbf{r}$ only if the vector $\mathbf{r} - \mathbf{r}_s$ is parallel to $\hat{\mathbf{n}}_0$, or

$$\mathbf{r} - \mathbf{r}_s = \alpha \hat{\mathbf{n}}_0, \tag{4.190}$$

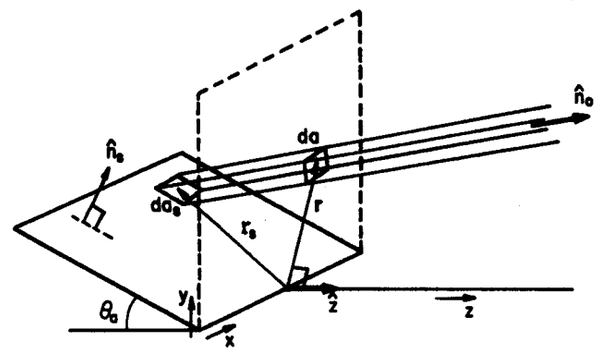

Fig. 4.29 Geometry for calculating the shift-variant PSF in transmission radiography with a tilted-anode x-ray tube.

where α is a scalar. Equations (4.189) and (4.190) can be satisfied simultaneously only if

$$\alpha = \frac{\mathbf{r} \cdot \hat{\mathbf{n}}_s}{\hat{\mathbf{n}}_0 \cdot \hat{\mathbf{n}}_s}, \tag{4.191}$$

from which we find

$$\mathbf{r}_s = \mathbf{r} - \left[\frac{\mathbf{r} \cdot \hat{\mathbf{n}}_s}{\hat{\mathbf{n}}_0 \cdot \hat{\mathbf{n}}_s}\right]\hat{\mathbf{n}}_0. \tag{4.192}$$

Thus $f(\mathbf{r})$ must be proportional to $L(\mathbf{r} - \alpha\hat{\mathbf{n}}_0, \hat{\mathbf{n}}_0)$. Two considerations are necessary to fix the constant of proportionality. The first is that $f(\mathbf{r})$ represents an emission into 4π steradians while $L(\mathbf{r}_s, \hat{\mathbf{n}}_0)$ represents emission into one steradian; a factor of 4π is therefore needed. The second point is that we must relate the area element d^2r in the plane $z = 0$ to the area element da_s in the actual source plane. This step is accomplished by projecting both da_s and d^2r onto a plane normal to $\hat{\mathbf{n}}_0$ and demanding that the projected areas be equal. In this way, all photons that are emitted by the element da_s in the direction $\hat{\mathbf{n}}_0$ must also pass through d^2r. This then requires that

$$(\hat{\mathbf{n}}_0 \cdot \hat{\mathbf{n}}_s)\, da_s = (\hat{\mathbf{n}}_0 \cdot \hat{\mathbf{z}})\, d^2r, \tag{4.193}$$

where $\hat{\mathbf{z}}$ is a unit vector parallel to the z axis and hence normal to the plane containing d^2r. But notice that $\hat{\mathbf{n}}_0 \cdot \hat{\mathbf{z}}$ is just $\cos\theta$ where, as before, θ is the angle between the z axis and the line along which the x rays travel. Similarly we define

$$\hat{\mathbf{n}}_0 \cdot \hat{\mathbf{n}}_s \equiv \cos\theta_s. \tag{4.194}$$

For the two functions $f(\mathbf{r})$ and $L(\mathbf{r}_s, \mathbf{n}_0)$ to describe the same emission patterns, we must have

$$L(\mathbf{r} - \alpha\hat{\mathbf{n}}_0, \hat{\mathbf{n}}_0)\, da_s\, d\Omega = f(\mathbf{r})\, d^2r\, d\Omega/4\pi \tag{4.195}$$

or, with (4.193) and (4.194),

$$f(\mathbf{r}) = 4\pi \frac{\cos\theta}{\cos\theta_s} L(\mathbf{r} - \alpha\hat{\mathbf{n}}_0, \hat{\mathbf{n}}_0). \tag{4.196}$$

Of course, $f(\mathbf{r})$ is now also a function of $\hat{\mathbf{n}}_0$ even though this dependence is not exhibited explicitly.

We shall illustrate this general result by returning to the disk focal spot of Section 4.3.1. In this case we assume that the high-energy electrons bombard a circular region on the anode, so that

$$L(\mathbf{r}_s, \hat{\mathbf{n}}_0) = L_0(\hat{\mathbf{n}}_0)\,\mathrm{circ}(2r_s/d_{fs}), \tag{4.197}$$

where $L_0(\hat{\mathbf{n}}_0)$ describes the angular dependence of the x-ray emission and is independent of $\mathbf{r}_s$. Equation (4.196) now becomes

$$f(\mathbf{r}) = 4\pi \frac{\cos\theta}{\cos\theta_s} L_0(\hat{\mathbf{n}}_0)\,\mathrm{circ}\left[\frac{2|\mathbf{r} - \alpha\hat{\mathbf{n}}_0|}{d_{fs}}\right]. \tag{4.198}$$

This expression for $f(\mathbf{r})$ describes an effective focal-spot distribution that is appropriate to those x rays that are emitted in the direction $\hat{n}_0$. Note that $f(\mathbf{r})$ is actually a very complicated function of $\hat{\mathbf{n}}_0$ since θ, θ_s, and α all depend on $\hat{\mathbf{n}}_0$. Moreover, α is a function of $\mathbf{r}$ also. However, the important features of the solution may be discerned by studying two special cases.

First, to verify that (4.198) is reasonable, suppose that the anode is actually parallel to the plane $z = 0$. Then $\theta_a = \pi/2$, $\mathbf{r} \cdot \hat{\mathbf{n}}_s = 0$, $\alpha = 0$, and $\theta_s = \theta$. The effective focal spot is then a simple circ function as expected:

$$f(\mathbf{r}) = 4\pi L_0(\hat{\mathbf{n}}_0)\,\mathrm{circ}(2r/d_{fs}) \qquad \text{if} \quad \theta_a = \pi/2. \tag{4.199}$$

Next we consider a general anode angle θ_a but assume that the object point lies on the z axis. The relevant vectors in component form are then

$$\begin{aligned} \hat{\mathbf{n}}_0 &= (0, 0, 1) \qquad \text{(object point on } z \text{ axis)}, \\ \hat{\mathbf{n}}_s &= (0, \cos\theta_a, \sin\theta_a), \\ \mathbf{r} &= (x, y, 0), \end{aligned} \tag{4.200}$$

from which, after a little algebra, we obtain

$$|\mathbf{r} - \alpha\hat{\mathbf{n}}_0| = [x^2 + (y^2/\sin^2\theta_a)^2]^{1/2}. \tag{4.201}$$

The circ function in (4.198) is nonvanishing within a region whose boundaries are determined by setting (4.201) equal to $d_{fs}/2$. This region is an ellipse with major axis d_{fs} and minor axis $d_{fs}\sin\theta_a$. In other words, the apparent dimension of the focal spot in the y direction is reduced by the factor $\sin\theta_a$, improving the resolution in that direction.

This same procedure can be used to find the shape of the effective focal spot for any object point. In all cases, it turns out to be an ellipse, but the algebra required to substantiate that statement is somewhat tedious. For this reason, and also because the disk focal spot is very artificial to begin with, the point will not be pursued further here.

We shall close this section by presenting a general expression for the shift-variant PSF in the tilted-anode geometry. To accomplish this end, we need to rewrite (4.196) in such a way that its $\mathbf{r}$ dependence is more evident. In particular, the $\mathbf{r}$ dependence of α must be exhibited. A useful vector identity here is the so-called **BAC–CAB** rule,

$$\mathbf{A} \times (\mathbf{B} \times \mathbf{C}) = \mathbf{B}(\mathbf{A} \cdot \mathbf{C}) - \mathbf{C}(\mathbf{A} \cdot \mathbf{B}), \tag{4.202}$$

which enables us to write

$$\mathbf{r} - \alpha\hat{\mathbf{n}}_0 = \frac{1}{\hat{\mathbf{n}}_0 \cdot \hat{\mathbf{n}}_s}[\mathbf{r}(\hat{\mathbf{n}}_0 \cdot \hat{\mathbf{n}}_s) - \hat{\mathbf{n}}_0(\mathbf{r} \cdot \hat{\mathbf{n}}_s)] = \frac{1}{\cos\theta_s}[\hat{\mathbf{n}}_s \times (\mathbf{r} \times \hat{\mathbf{n}}_0)]. \quad (4.203)$$

The shift-variant PSF is now found by substituting (4.196) and (4.203) into (4.54) and reinstating the $\cos^3\theta$ factor. The final result is

$$p_{fs}[\mathbf{r} - \mathbf{r}_0, \mathbf{r}_0] = 4\pi \frac{C}{a^2b^2} \frac{\cos^4\theta}{\cos\theta_s} L\left\{\frac{\hat{\mathbf{n}}_s \times [(\mathbf{r} - \mathbf{r}_0) \times \hat{\mathbf{n}}_0]}{-b\cos\theta_s}, \hat{\mathbf{n}}_0\right\}. \quad (4.204)$$

4.6.2 Septal Penetration

In this section we shall be concerned with photons that penetrate some distance through nominally opaque material and are detected when they should be blocked (Mather, 1957; Beck, 1968a,b). This phenomenon is more important in nuclear medicine than in diagnostic radiology for two reasons. First, gamma rays of interest in nuclear medicine are usually more energetic and hence more penetrating than diagnostic x rays. And second, the very act of image formation in nuclear medicine consists of blocking unwanted photons. Small amounts of penetration can thus be very important when compared to the small number of photons that are deliberately passed.

The first point to be made is that penetration can be described by *adding* a new term to the geometrical PSF calculated previously (Harris *et al.*, 1964; Beck, 1964b; Mather, 1957). This statement follows because all detected photons can be divided into two mutually exclusive classes: those that have penetrated through the nominally opaque material and those that did not encounter any opaque material in the first place. For a point source the detected photons of the latter class constitute the geometrical PSF of the previous sections. The photons of the former class produce another image which we shall call the *penetration PSF*.

The penetration PSF for a pinhole camera is easily calculated. Since it will generally be shift-variant we must fix the source point $\mathbf{r}_s$ and the observation point $\mathbf{r}''$ and then determine what path a photon must travel to get from $\mathbf{r}_s$ to $\mathbf{r}''$. If the path goes through the clear aperture of the pinhole, we are not interested since this photon contributes to the geometrical PSF rather than the penetration PSF. If, however, the path includes a thickness $t(\mathbf{r}'', \mathbf{r}_s)$ of absorbing material, we must calculate the probability that the photon will pass through the material unimpeded and go on to the detector. If the linear attenuation coefficient of the material is μ, this probability is simply $\exp[-\mu t(\mathbf{r}'', \mathbf{r}_s)]$. Scattering in the material can usually be neglected, especially if the detector is capable of energy discrimination.

As an example, consider a simple pinhole drilled through a lead plate of thickness t_0. For simplicity we assume that $s_1 = s_2$ and $t_0 \ll d'_{ph}$. If the plate is parallel to the detector, the path length $t(\mathbf{r}'', \mathbf{r}_s)$ is given by

$$t(\mathbf{r}'', \mathbf{r}_s) = t_0/\cos\theta(\mathbf{r}'', \mathbf{r}_s), \quad (4.205)$$

where, as before, $\theta(\mathbf{r}'', \mathbf{r}_s)$ is the angle of the ray measured from the normal to the detector plane. By a straightforward extension of the arguments given in Section 4.2, the penetration PSF is found to be [cf. (4.36)]

$$p_{pen}[\mathbf{r} - \mathbf{r}_s, \mathbf{r}_s] = C(b/a)^2 \exp[-\mu t_0/\cos\theta(\mathbf{r}'', \mathbf{r}_s)], \quad (4.206)$$

where $\mathbf{r} = -a\mathbf{r}''/b$, and the expression is valid everywhere except within the geometrical image of the pinhole. (If t_0 were comparable to the pinhole diameter, this expression would also be in error near the edge of the geometrical image.)

For penetration to be negligible the integral of $p_{pen}[\mathbf{r} - \mathbf{r}_s, \mathbf{r}_s]$ over the $\mathbf{r}$ plane must be small compared to the corresponding integral of $p_{ph}(\mathbf{r} - \mathbf{r}_s)$ given by (4.36). Roughly speaking, this requires that

$$\frac{\pi d_{det}^2}{4} \exp(-\mu t_0) \ll \frac{\pi d_{ph}^2}{4}\left(\frac{s_1 + s_2}{s_1}\right)^2. \quad (4.207)$$

Let us turn now to a somewhat more difficult problem—the calculation of the penetration PSF for a camera with a parallel-hole collimator. One effect of penetration in this case is to reduce the effective bore length. Even if the septa are very thick, gamma rays can still penetrate through the corners of the septa, thereby increasing the angular field of view of each individual bore. Since the mean penetration length is μ^{-1}, many authors make an approximate correction for this effect by replacing L_b with $L_b - \mu^{-1}$ in the equations for resolution, (4.165), and collection efficiency, (4.167). [In (4.165) this replacement applies only to the denominator. The numerator $L_s + L_b + z$ is the total distance from source to detector and is therefore constant.] Since μL_b must surely be large compared to unity in any usable collimator, this correction is a small one.

A more serious penetration problem occurs as the incidence angle is increased. Then the pathlength through any one septum decreases rapidly but the number of septa in the path increases correspondingly. The overall effect is to produce a broad, low-amplitude PSF very much as in the pinhole case.

A simple yet quite reasonable estimate of the total penetration can be obtained by just ignoring the fine structure of the collimator (Newell *et al.*, 1952). In other words, we imagine that the absorbing atoms are uniformly distributed through the volume of the collimator rather than arranged in discrete septa. The effective density of absorbing atoms is then given by the

actual density times $(1 - \alpha_{pf})$. This approximation is a poor one for small values of the incidence angle θ, but rapidly improves as θ is increased. At the extreme, if $\theta = 0$ then a photon can in reality penetrate a septum only by traversing the full bore length L_b; the probability of this occurrence is $\exp(-\mu L_b)$, a very small number. The model of a uniform distribution of absorber, however, predicts a probability of penetration at $\theta = 0$ of $\exp[-\mu L_b(1 - \alpha_{pf})]$. This is still a small number in practice, but is much larger than $\exp(-\mu L_b)$. The real justification for the model is that we are usually more interested in the total penetration, i.e., the integral of the PSF, than in the details of the shape of the PSF. Since the largest contribution to the integral will come from rays that cross several septa, the behavior near $\theta = 0$ is of little concern.

With these preliminaries we can now write down an expression for the penetration PSF of a parallel-hole collimator. By analogy with (4.206), we have

$$p_{pen}[\mathbf{r}'' - \mathbf{r}_s, \mathbf{r}_s] = T[4\pi(L_b + L_g + z)^2]^{-1} \exp\left[\frac{-\mu L_b(1 - \alpha_{pf})}{\cos\theta(\mathbf{r}'', \mathbf{r}_s)}\right]. \quad (4.208)$$

Once again, the penetration PSF is a broad, slowly varying function. To find the total penetration we must integrate (4.208) over the detector plane. This step can be carried out numerically or even analytically if a small-angle approximation for $\theta(\mathbf{r}'', \mathbf{r}_s)$ is valid.

Although such approximate techniques may give a useful indication of the penetration performance of a collimator for a scanner or camera, the only reliable way to get detailed information about penetration seems to be computerized ray tracing (Rotenberg and Johns, 1965; Jahns, 1981; Miracle *et al.*, 1979).

4.6.3 Patient Motion

Patient motion, an important practical problem in both diagnostic radiology and nuclear medicine, is easy to graft onto our formalism. As a highly idealized example, suppose the patient moves at constant velocity v during an exposure of time T taken with a scintillation camera. Then the image of a point is uniformly smeared over a line of length vT. We can describe this situation by a PSF for patient motion given by

$$p_{pm}(\mathbf{r}) = \frac{1}{vT}\,\mathrm{rect}\left(\frac{x}{vT}\right)\delta(y), \quad (4.209)$$

where $\mathbf{r} = (x, y)$ and the x axis is parallel to $\mathbf{v}$. The normalizing factor $1/vT$ ensures that $p_{pm}(\mathbf{r})$ approaches $\delta(\mathbf{r})$ if $v \to 0$. The overall system response is now found by convolving $p_{tot}(\mathbf{r})$, given by (4.174), with $p_{pm}(\mathbf{r})$.

Note that we did not specify above whether a pinhole, a parallel-hole collimator, or a magnifying or minifying collimator was used. It was not necessary to do so since we have been careful to refer all PSFs back to the original object scale. When a patient moves a distance vT, the corresponding PSF has width vT without need for any scale factors and without regard for the magnification of the rest of the system. Equation (4.209) is thus as applicable to projection radiography as it is to nuclear medicine.

One system that does behave somewhat differently with respect to patient motion is the scintillation scanner. In that case the effect of patient motion is better described as an image distortion rather than as a blur. Our previous example of a patient moving at constant velocity would result in a skewing of the scan raster in general. If $\mathbf{v}$ were parallel to the rapid-scan direction, the uniform patient motion would be exactly equivalent to an alteration of the scan velocity v_s. To take a more realistic example, suppose the patient moves during a single scan line and remains stationary during the remainder of the scan. Then the image would be distorted along that one line and unaffected elsewhere, although the sections of the scan taken before and after the motion would not necessarily match at their interface. Such a discontinuity is a common and easily identifiable sign of patient motion in scanner images.

Although patient motion is easy to treat analytically, it is not so easy to deal with in practice and, indeed, may often constitute the ultimate limitation to image quality. This is especially true if the motion is due to the natural cardiac and respiratory cycles. There are really only two possible ways to control image blur due to these movements. Either the exposure time can be made so short that no significant motion occurs, or "gated" imaging can be employed. One important example of the latter approach is gated liver imaging in nuclear medicine. Liver images are particularly susceptible to motion blur since the liver is adjacent to the diaphragm. However, if a transducer is used to monitor the patient's respiration, the scintillation camera can be electronically gated off except during the relatively quiet period of full expiration. Of course, total imaging time must then be increased to record the same number of total counts, but the image quality is significantly improved.

4.6.4 Three-Dimensional Objects

Our entire analysis so far has been a kind of "Radiology in Flatland" (Abbott, 1952). We have consistently described gamma-ray-emitting objects by a two-dimensional distribution of source activity, while objects of interest

in diagnostic radiology have been treated as absorbing planes. A full treatment of three-dimensional objects requires the methods developed in Chapters 7 and 9, but a few comments are presented here primarily in an effort to convince the reader that the foregoing sections of this chapter were more than an exercise in futility.

Consider first the nuclear medicine case where a three-dimensional object can be described by a three-dimensional source activity function, $f(\mathbf{r}, z)$. Here, $\mathbf{r}$ is still a two-dimensional vector in a plane a distance z from the collimator face or pinhole plane. A three-dimensional volume element is thus specified by $dv = d^2r\,dz$. The activity function is defined in such a way that $f(\mathbf{r}, z)\,d^2r\,dz$ is the number of photons per unit time emitted by material within the volume element $d^2r\,dz$ located at coordinates $(\mathbf{r}, z)$ or, equivalently, (x, y, z).

If the radiation were not appreciably absorbed within the patient's body, we could now use all of our previous results simply by replacing $f(\mathbf{r})$ with $f(\mathbf{r}, z)\,dz$ and then integrating over z. For example, (4.13) becomes

$$h(\mathbf{r}'') = T \int_0^\infty dz\,[4\pi(z + s_2)^2]^{-1} \int_\infty d^2r\, f(\mathbf{r}, z) g(a\mathbf{r}'' + b\mathbf{r}), \quad (4.210)$$

where

$$a = z/(z + s_2) \quad (4.211)$$

and

$$b = s_2/(z + s_2). \quad (4.212)$$

(Of course, z is identical to our previous parameter s_1, but the new designation emphasizes that it is a variable rather than a constant.)

However, (4.210) is not yet completely satisfactory because self-absorption may not be negligible. Furthermore, the body has very inhomogeneous attenuation properties, a fact that is essential to the success of diagnostic radiology but is a distinct nuisance in nuclear medicine. As discussed more fully in Chapter 7, a ray traversing this inhomogeneous medium is attenuated by a factor

$$\exp\left(-\int_S^D \mu(\mathbf{r}', z')\,dl'\right), \quad (4.213)$$

where $\mu(\mathbf{r}', z')$ is the linear attenuation coefficient at point $(\mathbf{r}', z')$, and the line integral runs from the source point S to the detector point D. Incorporating this factor in (4.210), we have

$$h(\mathbf{r}'') = T \int_0^\infty dz \int_\infty d^2r \frac{\exp\left(-\int_S^D \mu(\mathbf{r}', z)\,dl'\right)}{4\pi(z + s_2)^2} f(\mathbf{r}, z) g(a\mathbf{r}'' + b\mathbf{r}), \quad (4.214)$$

where the three-dimensional coordinates of S are $(\mathbf{r}, z)$. The important qualitative point about (4.214) is that calculation of the two-dimensional image $h(\mathbf{r}'')$ in general requires the knowledge of two separate three-dimensional distributions, $f(\mathbf{r}, z)$ and $\mu(\mathbf{r}, z)$.

Often it is valid to replace $\mu(\mathbf{r}, z)$ in (4.214) by a constant. For example, if only soft tissue intervenes between S and D, it is quite reasonable to replace $\mu(\mathbf{r}, z)$ by μ_{H_2O}, the attenuation coefficient of water. This approximation does not, however, completely circumvent the problem since the path length from S to D depends on $\mathbf{r}$, z, and the external contours of the patient's body. Perhaps the best that can be said in general is that a nuclear medicine image does not really measure $f(\mathbf{r}, z)$, but rather $f(\mathbf{r}, z)\exp(-\int_S^D \mu\,dl)$. The exponential factor may or may not approximate a constant, depending on photon energy, depth of the organ being imaged and obesity of the patient. For example, a lung scan of a plump woman may show regions of apparently reduced activity due entirely to absorption in the breasts. On the other hand, if a liver scan is performed with a parallel-hole collimator on a slender patient, it would be very reasonable to regard the exponential factor as a constant multiplier for each plane z. And finally, for high-energy photons such as the 360-keV gamma rays from ^{131}I and superficial organs like the thyroid, very little error is made in ignoring absorption altogether.

The problem of three-dimensional objects becomes even more untidy in the transmission radiography case. If we represent a volume absorber by a stack of N absorbing planes, the generalization of (4.13) is

$$h(\mathbf{r}'') = C \int_\infty d^2r\, f(\mathbf{r}) \prod_{i=1}^{N} g_i(a_i\mathbf{r}'' + b_i\mathbf{r}), \quad (4.215)$$

where $g_i(\mathbf{r}')$ is the transmission of the ith plane at point $\mathbf{r}'$,

$$a_i = 1 - b_i = \frac{z_i}{z_i + s_2}, \quad (4.216)$$

and z_i is the distance of the ith plane from the source plane.

Equation (4.215) is most easily interpreted if the focal-spot distribution can be approximated by a delta function,

$$f(\mathbf{r}) \approx f_0\,\delta(\mathbf{r}), \quad (4.217)$$

in which case,

$$h(\mathbf{r}'') = Cf_0 \prod_{i=1}^{N} g_i(a_i\mathbf{r}''). \quad (4.218)$$

In other words, the measured image $h(\mathbf{r}'')$ consists of a *multiplicative* (and hence nonlinear) superposition of images of each of the planes, with the magnification for the ith plane given by $1/a_i$.

When a screen-film system is used as the image detector, a further simplification is possible. As discussed in Chapter 5, the optical density D in the developed film is usually a linear function of the logarithm of the exposure, i.e.,

$$D(\mathbf{r}'') = D_0 + \gamma \log[h(\mathbf{r}'')], \tag{4.219}$$

where D_0 and γ are constants characteristic of the film. The logarithm converts the multiplicative superposition of (4.218) into an additive one:

$$D(\mathbf{r}'') = D_0 + \gamma \log(Cf_0) + \gamma \sum_{i=1}^{N} \log[g_i(a_i\mathbf{r}'')]. \tag{4.220}$$

In a peculiar sense, then, we have salvaged the linear systems approach to transmission radiography even with three-dimensional objects. We need only to regard the logarithm of the transmission, rather than the transmission itself, as the input to the system and to regard the optical density $D(\mathbf{r}'')$ as the output to obtain a linear input–output relation.

Of course, all of this was possible only because we assumed a delta-function source. The situation is far more complicated when we have a general source function and a three-dimensional (or multiplanar) object. Without really attempting a full solution, we can suggest the nature of the difficulty by rewriting (4.215). Suppose we are interested in one particular plane, say the jth. Then the factors in the N-fold product in (4.215) can be regrouped as

$$h(\mathbf{r}'') = C \int_{\infty} d^2r \left(f(\mathbf{r}) \prod_{i \neq j}^{N} g_i(a_i\mathbf{r}'' + b_i\mathbf{r}) \right) g_j(a_j\mathbf{r}'' + b_j\mathbf{r}). \tag{4.221}$$

The point spread function appropriate to the jth plane is calculated as in Section 4.3 by letting $g_j(\mathbf{r}')$ be a delta function,

$$g_j^{\delta}(\mathbf{r}') = \delta(\mathbf{r}' - \mathbf{r}_1). \tag{4.222}$$

The resulting image is given by

$$h^{\delta}(\mathbf{r}'', \mathbf{r}_1) = \left(\frac{C}{b_j}\right) f\left[\frac{\mathbf{r}_1}{b_j} - \frac{a_j\mathbf{r}''}{b_j}\right] \prod_{i \neq j}^{N} g_i\left(a_i\mathbf{r}'' + \frac{b_i}{b_j}(\mathbf{r}_1 - a_j\mathbf{r}'')\right). \tag{4.223}$$

In other words, the PSF is determined not only by the actual source function $f(\mathbf{r})$, but also by the details of the absorbing structures in all other planes. For example, a sharp-edged absorber in one plane can partially obscure the focal spot for some values of $\mathbf{r}'$ and hence improve the apparent system resolution. The PSF is, of course, highly shift-variant because of parallax among the various planes.

One important limit should be mentioned. When the three-dimensional object is relatively structureless and has low contrast (e.g., soft tissue), then the effect of the product term in (4.223) is merely to modulate the overall intensity of the source distribution without seriously affecting the details of its shape. The imaging system is still shift-variant, but a relatively large isoplanatic patch can be defined. In this case we are justified in using the planar models of Section 4.3 to calculate PSF, MTF, etc.